Compression behaviour of steel fibre reinforced self-compacting concrete – age influence and modeling

Vítor M.C.F. Cunha,
Joaquim A.O. Barros, José M. Sena-Cruz

Report 06-DEC/E-04

Date: January 2006
No. of pages: 49

Keywords: Steel fibre reinforced self-compacting concrete; Compression; Stress – strain curve; Age (of concrete); Analytical model.

School of
Engineering

Department of
Civil Engineering

University
of Minho

Azurém, 4800-085 Guimarães, Portugal
Tel. (+351) 253 510 200 – Fax (+351) 253 510 217 – Email: secG@civil.uminho.pt

Acknowledgments

The study reported in this paper is part of the research program "*Prefabricated sandwich steel fiber reinforced panels*" supported by FEDER and MCT, and promoted by ADI (the funds were 45% of the applied amount). This project involves the Companies PREGAIA and CIVITEST, and the University of Minho. The authors wish to acknowledge the materials generously supplied by Bekaert (fibers), SECIL (cement), Degussa (superplasticizer), and Comital (limestone filler). The first author wishes also to acknowledge the grant SFRH/BD/18002/2004, provided by FCT.

Contents

List of Figures

List of Tables

Chapter 1

Introduction

1.1 Introduction

The use of steel fiber reinforced self-compacting concrete, SFRSCC, probably, will swiftly increase in the next years, since this composite material introduces several advantages on the concrete technology. In fact, the partial or total replacement of the conventional bar reinforcement by discrete fibers optimizes the construction process. The assembly of the reinforcement bars in the construction of concrete structures has a significant economical impact on the final cost of this type of constructions, due to the man-labor time consuming that it requires. In the modern societies, the cost of the man-labor is significant, from which diminishing the man-labor will decrease the overall cost of the construction. For this reason, SFRSCC is a very promising construction material with a high potential of application, mainly in the cases where fibres can replace the conventional reinforcement. At the present time, however, the SFRSCC technology is not yet fully developed and controlled, and, much less, the mechanical behavior of the SFRSCC material.

In the fresh state, SFRSCC homogeneously spreads due to its own weight, without any additional compaction energy. To homogeneously fill a mould, SFRSCC has to fulfill high demands with regard to filling and passing ability, as well as segregation resistance. Driven by its own weight, the concrete has to fill a mould completely without leaving entrapped air even in the presence of dense steel bar reinforcement. All the concrete components have to be homogeneously distributed during the flow and at rest (Grünewald, 2004).

The most benefited properties with the fiber addition to the concrete, in the hardened state, are the impact strength, the toughness and the energy absorption capacity. A detailed description of the benefits provided by the fiber addition to concrete can be found elsewhere, (Balaguru and Shah, 1992; Casanova, 1996; ACI 544.1R, 1997). The fiber addition might also improve the fire resistance of cement-based materials (Kodur and Bisby, 2005), as well as the shear

resistance (J. Rosenbusch and M. Teutsch, 2003). Recently, Grünewald (2004) compared the mechanical behavior of SFRSCC to the behavior of current fiber reinforced concrete, FRC. This author carried out bending and pull-out tests, and concluded that those properties were much better in the SFRSCC.

The field of possible application of SFRSCC include: highways, industrial and airfield pavements; hydraulic structures, tunnel segments, bridges components and concrete structures of complex geometry which present high difficulties of being reinforced by conventional steel bars, especially those who have high degree of support redundancy.

Available material models are not able of simulating, with sufficient accuracy, the behavior of SFRSCC, which requires that more research should be done in this domain. A good knowledge of the stress-strain relationship at early ages plays an important role in the determination of time for the removal of shoring and in the calculation of thermal stresses due to the hydration heat of cement and shrinkage stresses that occur during the hardening. A comprehensive understanding of the behavior of concrete members at an early age is necessary not only for the design and construction of the concrete structures but also for the evaluation of durability and service life. Moreover, in the precasting industry, demoulding the elements as soon as possible is an important requirement. To assure safe demoulding process, the influence of the concrete age on the compression behavior of the SFRSCC should be known.

The stress-strain relationship, $\sigma_c - \varepsilon_c$, representing the behavior of a material under uniaxial compression, is an important material characteristic of concrete. However, due to various influencing factors and different experimental conditions, distinct $\sigma_c - \varepsilon_c$relationships are available. Most model equations used presently have been developed for old-age concrete and for plain (Carreira and Chu, 1985; CEB – FIP, 1993) and current fiber reinforced concrete (Ezeldin and Balaguru, 1992; L. S. Hsu and C. T. Hsu, 1994). In the context of SFRSCC, there are not appropriate stress-strain equations to model the early age concrete behavior under compression.

This report is the continuity of a research program for the development of lightweight sandwich SFRSCC panels for precasting industry. The requirements established for this SFRSCC were the following: average compression strength at 24 hours greater than 20 MPa; equivalent flexural tensile strength greater than 2 MPa at this age; content of cement not exceeding 400 kg/m^3 (Pereira *et al.*, 2004, 2005). In this work, the compressive softening behavior of SFRSCC was investigated, within a structural point of view. Stress-strain laws are proposed to model the behavior of the SFRSCC since the early ages. Additionally empirical expressions to predict the principal mechanical properties are presented.

Chapter 2

Experimental programme

2.1 Research parameters

The present experimental program was defined to evaluate the influence of the fiber content and concrete age on the direct behavior of steel fiber reinforced self-compacting concrete, SFRSCC.

For this purpose, two series of distinct fiber contents were prepared. The first one with 30 kg/m^3 is denominated by *Cf30* and, the other, with 45 kg/m^3 designated by *Cf45*. Each of these series was composed by subseries that were tested at 12 and 24 hours, 3, 7 and 28 days.

The stress-strain relationship was obtained as the direct result of the compression tests. Additionally, the principal mechanical properties of the SFRSCC, such as: the compressive strength, f_{cm}, the elasticity modulus, E_{ci}, strain at peak stress, ε_{cp} and the volumetric energy dissipated, G_c were also determined.

2.2 Concrete mixture

2.2.1 Conception method

The materials used in the composition of the steel fiber reinforced self-compacting concrete, SFRSCC, were: cement (C) CEM I 42.5R, limestone filler (LF), superplasticizer (SP) of third generation based on polycarboxilates (Glenium® 77SCC), water (W), three types of aggregates (fine river sand (FS), coarse river sand (CS) and crushed granite 5-12 mm (CA)) and DRAMIX® RC-80/60-BN hook-ended steel fibers. The adopted fiber had a length (l_f) of 60 mm, a 0.75 mm diameter (d_f), an aspect ratio (l_f/d_f) of 80 and a yield stress of 1100 MPa (Dramix, 1998).

In previous works (Pereira *et al.*, 2004, 2005) a series of tests were carried out to achieve the optimum composition. The method used for defining the composition of the SFRSCC was

based on the three following steps:

1. the proportions of the constituent materials of the binder paste were defined;
2. the proportions of each aggregate on the final solid skeleton were determined;
3. binder paste and solid skeleton were mixed in different proportions until self-compacting requirements in terms of spread ability, correct flow velocity, filling ability, blockage and segregation resistance were assured.

In the first step, a series of tests were performed to achieve the optimum composition of the binder paste. To define the optimum percentage of LF addition in the final composition, several mixes of LF, cement and water were executed. The proportions of each component were defined in terms of volume, the water content was 66% of cement volume, and the percentage of LF has varied between 0% and 125% of the cement volume. To promote the dispersion and deflocculation of the fine particles in suspension, a small constant quantity of superplasticizer was also added to each mix. The relative spread in the "Flow table" and the "Marsh cone" flow time of each mix were measured. To give some guidance in the paste phase design, the compressive strength of each mix was also evaluated on 5 cm edge cubic specimens at an age of 7 days. A percentage of LF similar to the cement percentage has resulted in a good compromise between strength and flowability requirements, and has also allowed maintaining the amount of cement on the final concrete mix only slightly above 350 kg/m^3 for the *Cf30* series.

In the second step, the most appropriate proportions of the three types of aggregates were obtained executing mixes of distinct quantities of each type of aggregate, and weighting 5 dm^3 volume for each mix. The optimum aggregate mix was assumed to be the heaviest one, since it should correspond to the most compact. An estimated portion of fibers equivalent to 30 kg of fibers per m^3 of concrete was included in every mixture. Initially, only two of the three types of aggregates were mixed. After finding the optimum relation between these two, the third aggregate was added in distinct volumetric percentages, keeping constant the relation between the two first aggregates. These results indicated that the optimum solid skeleton was composed, in volume, by 49.5% of coarse sand, 40.5% of crushed stone and 10% of fine sand for the *Cf30* series.

Relatively to the *Cf45* series, since a higher content of fibers is used, the solid skeleton composition (aggregates) should be redesigned to avoid an increase of void content in the solid skeleton structure. The solid skeleton composition was evaluated according to the procedure previously described. The final composition of the solid skeleton for *Cf45* series was (in percentage of volume): 46.75% of coarse sand, 38.25% of crushed aggregate and 15% of fine sand. Note that the percentage of fine sand increased, while the relative percentage of coarse sand

and crushed aggregate decreased. To obtain the percentage of the binder paste in the total volume of concrete, some mixes of concrete were conceived, varying the paste percentage. To attain the self-compacting requirements for the series with a content of fiber of 45 kg/m^3, when compared to *Cf30* series, it was necessary to increase the ratio of paste / total volume, as well the volume of the superplasticizer. The self compacting parameters were measured for each trial, performing the L-Box and the Slump Flow tests. In this phase the V-Funnel test was not used. In fact, this test is not feasible since the fiber has a too high length for the reduced overture of the apparatus of this test.

Table 2.1 includes the composition that has best fitted self-compacting requirements for the two contents of fibers (Cf) adopted, 30 and 45 kg/m^3. Remark that, in Table 2.1, WS is the water necessary to saturate the aggregates and W/C is the ratio water/cement. The parcel WS was not used to compute the ratio W/C.

Table 2.1: Final composition for 1 m^3 of SFRSCC.

Cf (kg)	Paste/Total volume (%)	Cement (kg)	LF (kg)	Water (dm^3)	WS (dm^3)	SP (dm^3)	FS (kg)	CS (kg)	CA (kg)	W/C
30	0.34	359.4	312.2	96.9	64.7	6.9	108.2	709.4	665.2	0.29
45	0.38	401.7	344.3	108.4	60.8	7.6	101.7	666.4	624.8	0.29

2.2.2 Mixing

A planetary mixer of vertical axis, of 360 l capacity was used to manufacture the SFRSCC. In each series, approximately 250 liters were produced. For every mixture, fine and coarse river sand, crushed granite, water, cement, limestone filler and the steel fibers were weighed separately. The accuracy of the weighting device for the aggregates was about 10 g, whereas for the other items the accuracy of the weighting device was about 1 g.

The aggregates were put into the mixer in a predetermined order. First the crushed granite was added, then the coarse river sand and the fine river sand, and finally were mixed during one minute. Meanwhile, the aggregate saturation degree was determined. After this, it was added the necessary water quantity to saturate the aggregates (WS), and the mixing continued again during one minute. Then, by this order, the limestone filler and cement were added, and another minute of mixing was taken. Afterwards, the water necessary to hydrate the cement was added with the mixing machine running, finally the superplasticizer and the steel fibers were added. The concrete was mixed during about 300 seconds, until it started to exhibit good homogeneity.

After mixing the concrete and before casting, the following properties were measured: flow spread and flow rate.

2.2.3 Properties of the fresh concrete

Figure 2.1 depicts the final state of a performed slump flow test for a self-compacting concrete with 45 kg/m^3 of fibres. No sign of segregation was detected. A total spread of over 700 mm was measured for both series, and the mixture showed good homogeneity and cohesion, even when flowing through the small orifice of the Abrams cone. Notice that when testing, the Abrams cone was always used in the inverted position.

Another parameter measured was the time to reach a spread diameter of 500 mm, T_{50}. For the series with 30 kg/m^3, T_{50} was 4.5 seconds, whereas for series with 45 kg/m^3 a time of 5.2 seconds was measured.

Figure 2.1: Self-compacting concrete spread obtained on the slump flow test for a self-compacting concrete with 45 kg/m^3 of fibres.

2.3 Test specimens

The recommendation of RILEM TC 148-SSC (2000), for strain-softening tests under uniaxial compression, requires at least three test specimens per experiment. In the present work, six specimens were used for each series. This number of specimens was chosen to take the scatter into account, in order to obtain a more realistic average result.

2.3.1 Dimensions

Several authors recommend a minimum test specimen size according to the dimension of the aggregate, or in the present case, the fiber length. Kooiman (2000) and RILEM TC 148-SSC (2000) suggested that the minimum dimention of the test specimen should be at least five times the largest aggregate. On the other hand, the ACI Committee 544 (1988) recommend that the smallest specimen dimension should be three times larger than the fiber length and/or the maximum aggregate size. In the present work, fibers with a length of 60 mm were used, which suggests that the minimum test specimen size should be 180 mm or 300 mm according to the previous recommendations.

To have a representative zone that is not influenced by the confinement effect introduced by the steel load platens of the compression machine into the concrete (Mier, 1984, 1997), the specimen should a length larger than twice the characteristic dimension of its cross section (RILEM TC 148-SSC, 2000; Camões, 2002).

If a cylinder specimen is adopted, the previous recommendations point out the use of a specimen with a diameter of 180 mm and a length of 360 mm, or a specimen of 300 mm diameter and 600 mm length. If this last specimen was adopted, the number of specimens for each batch would have to be smaller than the desired number, due to the volume capacity of the mixer. Since fibrous distribution increases the dispersion of the main relevant concrete properties, the minimum number of specimens, previously indicated, should be a priority requisite on the decision of selecting the specimen dimensions. Since the dimensions of the smallest possible specimen are not too different of the cylindrical molds available in the laboratory, 150 mm diameter and 300 mm height cylindrical specimens were adopted for the assessment of the compression behavior of the designed SFRSCC.

2.3.2 Production

The test results are affected by the way that the specimens are obtained and tested (Mier, 1997). In fact, the relative direction between the concrete casting and the test loading, and the method for obtaining the specimens *sawingorcasting* are some of the conditions that affect the stress-strain relationship recorded in the tests. This can be aggravated in the fibrous concrete specimens, since the type of mould, the casting method and the type of compaction affect the fiber orientation and fibre distribution into concrete and, consequently, different responses will be obtained.

According to the RILEM TC 148-SSC (2000) recommendation to determine the strain softening behavior of plain concrete under uniaxial compression, there are two possibilities to manufacture the test specimens: casting them directly in the size required for the tests,

or sawing them from larger blocks. The first alternative is preferred in the present work. This recommendation also suggests that cylinders must be casted vertically and the specimen top surface must be ground in order to assure that the specimen extremities are parallel and orthogonal to the specimens axis.

Due to the smaller resistance of the test specimens for recent ages (12 and 24 hours), a cap of a self-leveling high resistance mortar was applied on the surface of specimen extremities in detriment of the surface grind procedure. In the test specimens of 3, 7 and 28 days the parallelism of the specimen end surfaces was assured by the grind procedure.

The totality of specimens were casted without any external compaction energy.

2.3.3 Curing and demoulding

After specimens having been casted, they were covered with a wet cloth to avoid moisture losses and were left in the laboratory until the day of the tests. During this period the cloth was maintained soaked. This procedure was adopted by the fact that, due to the large quantity of specimens, they could not be all put in the fog room at 99% RH and 20°C as recommended by RILEM TC 148-SSC (2000). However, since the specimens were all the time covered by a wet cloth, the relative humidity value should be nearby the value recommended by RILEM TC 148-SSC (2000) according to the RILEM TC 148-SSC (2000). The average temperature in the laboratory, during the experimental program for the series with a fiber content of 30 kg/m^3 was approximately 15°C, while for the series with 45 kg/m^3 of fibers was 20°C, which are not to distinct to the value recommended by RILEM TC 148-SSC (2000). The specimens were demoulded in the test day.

2.4 Test set-up

The compression tests, for obtaining the elasticity modulus and the stress – strain relationship were carried out in a servo-controlled equipment of 3000 kN maximum load carrying capacity.

2.4.1 Elasticity modulus

The determination of the elasticity modulus was performed according to the LNEC E397 (1993) Portuguese standard. Other standards, such as RILEM TC 14-CPC (1975) and ASTM C469 (1994) recommend similar procedures to those proposed by LNEC E397 (1993). According to this specification the test should be carried out under force control over a certain number of cycles. The test ends when the strain difference, between two consecutive loading cycles, does not exceed 1×10^{-5}. In the initial phase of the test, a stress of 0.5 MPa (σ_b) is applied, and the

corresponding strain is measured ε_b. The stress is than increased at a velocity of 0.2 MPa/s until a stress level $\sigma_a = f_c/3$ is attained, where f_c is the compressive strength, previously obtained in a direct compression test. The stress σ_a is maintained during 90 seconds, and in the last 30 seconds of this period, the strains are recorded ε_a. After this period, the load is decreased at a stress ratio of 0.2 MPa/s until a stress level σ_b. This stress level is maintained during a period of 90 seconds, and in the last 30 seconds of this period, the strains are recorded. The elasticity modulus is the average of the $E_{c,n}$ values obtained in each cycle:

$$E_{c,n} = \frac{\Delta\sigma_n}{\Delta\varepsilon_n} = \frac{\sigma_{a,n} - \sigma_{b,n}}{\varepsilon_{a,n} - \varepsilon_{b,n}} \tag{2.1}$$

where $\sigma_{a,n}$ and $\sigma_{b,n}$ are the average of the two stress limits of the n^{th} cycle, $\varepsilon_{a,n}$ and $\sigma_{b,n}$ are the correspondent strains. The measurement of the axial displacement was accomplished using three linear voltage displacement transducers, *LVDT's*, placed in such a way as depicted in Figure 2.2. The distance between the two rings should be greater than the length of the specimen edge or diameter with a minimum value of 100 mm. The distance between the two rings adopted in the tests was 100 mm. The ring device was positioned mid height of the specimen.

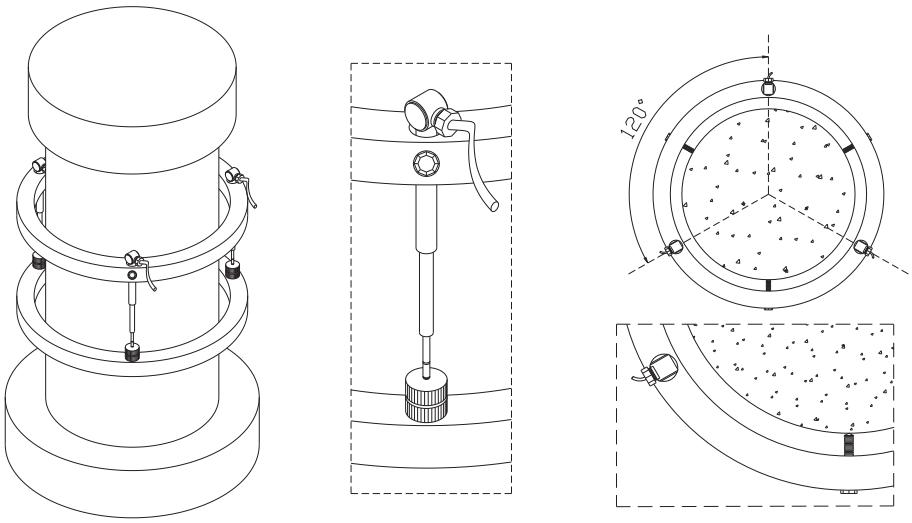

Figure 2.2: Setup of the compression test to obtain the elasticity modulus.

2.4.2 Stress-strain curve

To obtain the entire stress – strain curve, $\sigma_c - \varepsilon_c$, demands that the tests overpass the peak stress and should be only ended when the residual stress in the post peak $softeningphase$ is a

smaller percentage of the peak stress. To assure stable tests in the softening phase the testing equipment should have enough stiffness and sophisticated PID control should be available. The used testing rig has these features and the tests were carried out in displacement control.

During the test, the strains were obtained from the relative displacement of the loading platens. For this purpose three *LVDT's* were disposed around the test sample forming an angle of 120 degrees between consecutive *LVDT's*. Figure 2.3 shows the adopted test scheme. This test set up avoids that the deformation of the test equipment is added to the displacements read by the *LVDT's*. This arrangement of the transducers also allows that the specimen deformation in the longitudinal axis, can be computed simply by the average readouts of the three transducers. There is no need to attend to the rotation of the upper loading paten, since the computed deformation is at the longitudinal axis of the specimen. The strain was calculated from the average displacement readings divided by the height of the specimen.

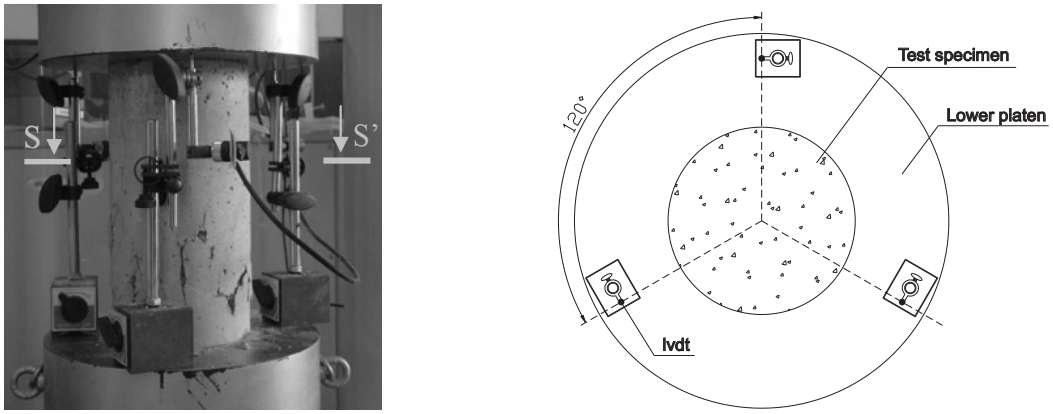

(a) (b)

Figure 2.3: Setup of the compression test to obtain the stress-strain curve: a) general view, b) section s–s'.

According to RILEM TC 148-SSC (2000), the uniaxial compression test of plain concrete should be carried out with a displacement ratio of 1 $\mu m/s \pm 0.1$ $\mu m/s$. However, for steel fiber reinforced concrete $SFRC$, the tests can be performed with higher displacements ratios. The Japanese recommendation JSCE – SF4 (1984) suggests displacements ratios between the 10 $\mu m/s$ and 30 $\mu m/s$, for the uniaxial compression tests on SFRC specimens. According to Barros (1995) the stability of the compression test on SFRC specimens is guaranteed for those displacement ratios. In the present work, the compression test was carried out using two distinct displacement ratios, up to a deformation of 5 mm, a displacement ratio of 10 $\mu m/s$ was

used, while the remaining test phase was controlled at a displacement ratio of 30 $\mu m/s$. The test ended at a deformation of 20 mm.

Chapter 3

Experimental results

3.1 Failure modes

The typical failure modes observed in the specimens tested under uniaxial compression are schematically represented as the projection to the longitudinal symmetry plane of the cylinder, and are depicted in Figure 3.1.

In the tested specimens two distinct failure modes, *FM1* and *FM2* were visualized. The third failure mode, *FM3*, was very similar to *FM1*, however larger volume of concrete at the specimen bottom zone was maintained with marginal damage on the specimens pulled according to *FM1* mode. An eventual fiber concentration in the specimen bottom part can justify this failure mode. The *FM1* failure mode is characterized by the formation of two cones on the extremities of the cylinder, whereas in the central zone there was the formation of compressive struts separated by vertical cracks. The central part of the cylinder and the cones were not detached due to the fibers bridging the cracks, which assured the stress transfer between the rupture surfaces.

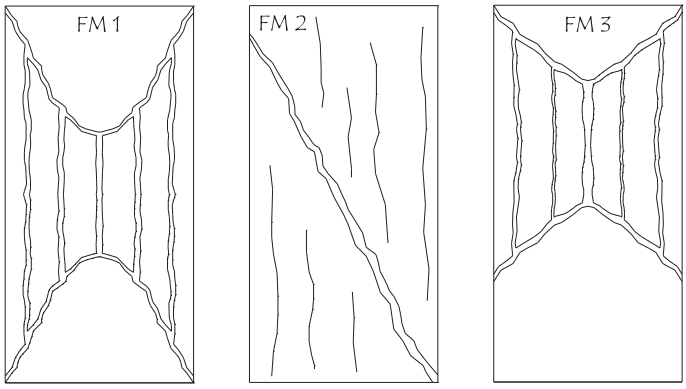

Figure 3.1: Scheme of the failure modes observed in the uniaxial compression tests.

In the specimens failed in *FM2* mode, after the formation of the vertical cracks, which were visible just before the peak load, a shear failure crack was formed in the beginning of the softening phase. The opening and the sliding of this shear failure crack have augmented up to the end of the test. In general, this failure mode leads to stress-strain responses of high volumetric energy, mainly in the softening phase. This can be justified by the fracture mode I energy dissipated in the crack opening process of the cracks positioned in the vertical (or quasi-vertical) direction (G_{fI}), and the fracture mode I and II energies dissipated in the opening (G_{fI}) and sliding (G_{fII}) of the faces of the shear failure crack (see Figure 3.2). Since the fibers bridging this shear cracks offer resistance to crack opening, the energy dissipated for sliding the faces of this crack increases (higher effect of aggregate interlock).

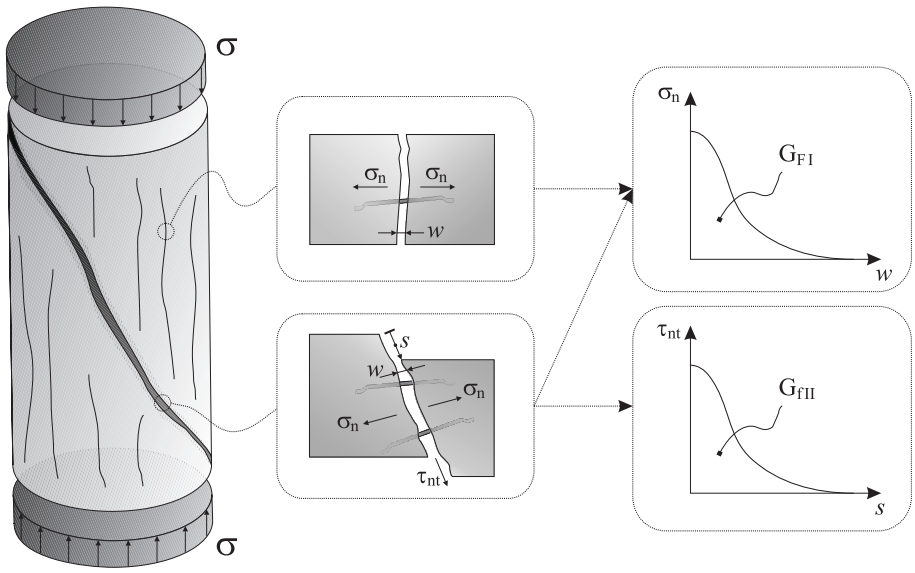

Figure 3.2: Fibre reinforcement mechanisms in failure mode *FM2*.

Finally, the *FM3* failure mode developed a smaller cone on the top part of the specimen, whereas the bottom part had little damage. As already mentioned, the higher fiber concentration in the specimen bottom part can justify the reduced damage verified in the almost bottom half part of the specimen. The confinement provided by this zone has forced the vertical compressive struts to propagate into the zone where a cone of confined concrete is formed due to the friction between the top steel platen of the equipment and the top specimen extremity. In result, the height of this cone become smaller. An eventual lower content of fibers in the top part of the specimen can also have contributed for the decrease of the dimension of this concrete cone.

Table 3.1 indicates the failure modes observed in each series. The confinement provided by

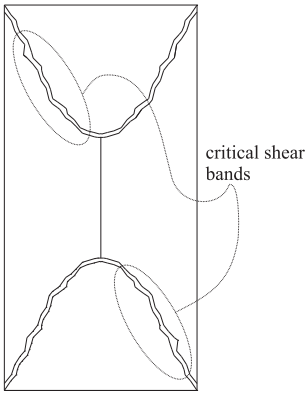

Figure 3.3: Critical shear bands.

the machine steel platens and the existence of fiber reinforcement leads to two zones, at the specimens extremities, of bigger resistance to the crack propagation into these zones. In plain concrete of moderate and low strength concrete, each one of these zones, generally, degenerates into conical geometry. However, in high strength fibrous concrete, the fiber pull out resistance is much higher than the resistance offer by the fibers to the crack sliding. In result, when these high confined concrete zones are displaced due to the applied load, the principal stresses in the contour of these zones are inclined forming inclined micro-cracks that degenerate into a shear failure crack band (see Figure 3.3). This justifies why only *FM2* failure mode have occurred in the high strength concrete series (3,7 and 28 days), while *FM1* and *FM3* failure modes were visible in the remaining series.

Table 3.1: Observed failure modes.

Age	Series	
	Cf30	*Cf45*
12 hours	*FM2*, *FM3*	*FM2*, *FM3*
24 hours	*FM1*, *FM2*	*FM2*, *FM3*
3 days	*FM2*	*FM2*
7 days	*FM2*	*FM2*
28 days	*FM2*	*FM2*

The specimens of the series with 3, 7 and 28 days, which in these series presented a lower toughness under compression, had a smaller number of fibers crossing the rupture surface. Figure 3.4 shows two specimens with a rupture mode by shear containing distinct amount of fibers crossing the rupture surface. A closer analysis to the fibers on the rupture surface showed that they did not fail, and in general the hooked end of the fibers was stretched, which means that the pull out resistance of these fibers were effectively activated.

(a) (b)

Figure 3.4: Shear rupture surface: (a) with fibers and (b) without fibers (image edited).

3.2 Stress-strain relationships

The stress-strain curves, $\sigma_c - \varepsilon_c$, for the series *Cf30* and *Cf45* are represented in Figures 3.5 and 3.6, respectively.

A larger non-linear branch can be observed in the pre-peak behavior of the specimens of 12 and 24 hours. In fact, a pronounced nonlinear behavior is observed in the pre-peak phase due to the aggregates – paste weak bond at this age. The porous structure of the interface is gradually converted into discontinuous microcracks and, finally, into continuous cracks during the strain increment applied to the specimens. Since the stiffness of the paste is relatively low at these satges, this damage evolutive procedure is much more stable than in older specimens. Consequently, a smother residual strength decay has occurred in the softening phase of the 12 hours specimens. At this age, the energy dissipated by the pullout of the fibers after crack initiation is only a small part of the energy at older ages, since the bond strength and the stiffness of the fiber-concrete interface is still relatively low at this age. Throughout the concrete aging, the interface and the paste become more stiff, resulting in a $\sigma_c - \varepsilon_c$ linear relationship of higher amplitude in the pre-peak phase. This stiffening and strengthening gaining process leads to more brittle responses in the post-peak phase.

Since the fibers crossing the cracks did not break, the concrete energy absorption capacity would have increased with the content of fibers added to the mixture. However, this was not evidenced in the present research, which can be justified by the decrease of the compressive strength from series *Cf30* to *Cf45*, that caused a decrease in the fiber – concrete bond strength and, consequently, a decrease in the energy dissipated in the fiber pull-out process. The decrease of the compressive strength from series *Cf30* to *Cf45* might be justified by the higher w/c ratio and LF percentage, as well as the lower content of coarse aggregate and coarse sand.

The average $\sigma_c - \varepsilon_c$ curves are depicted in Figure 3.7. The average compressive strength

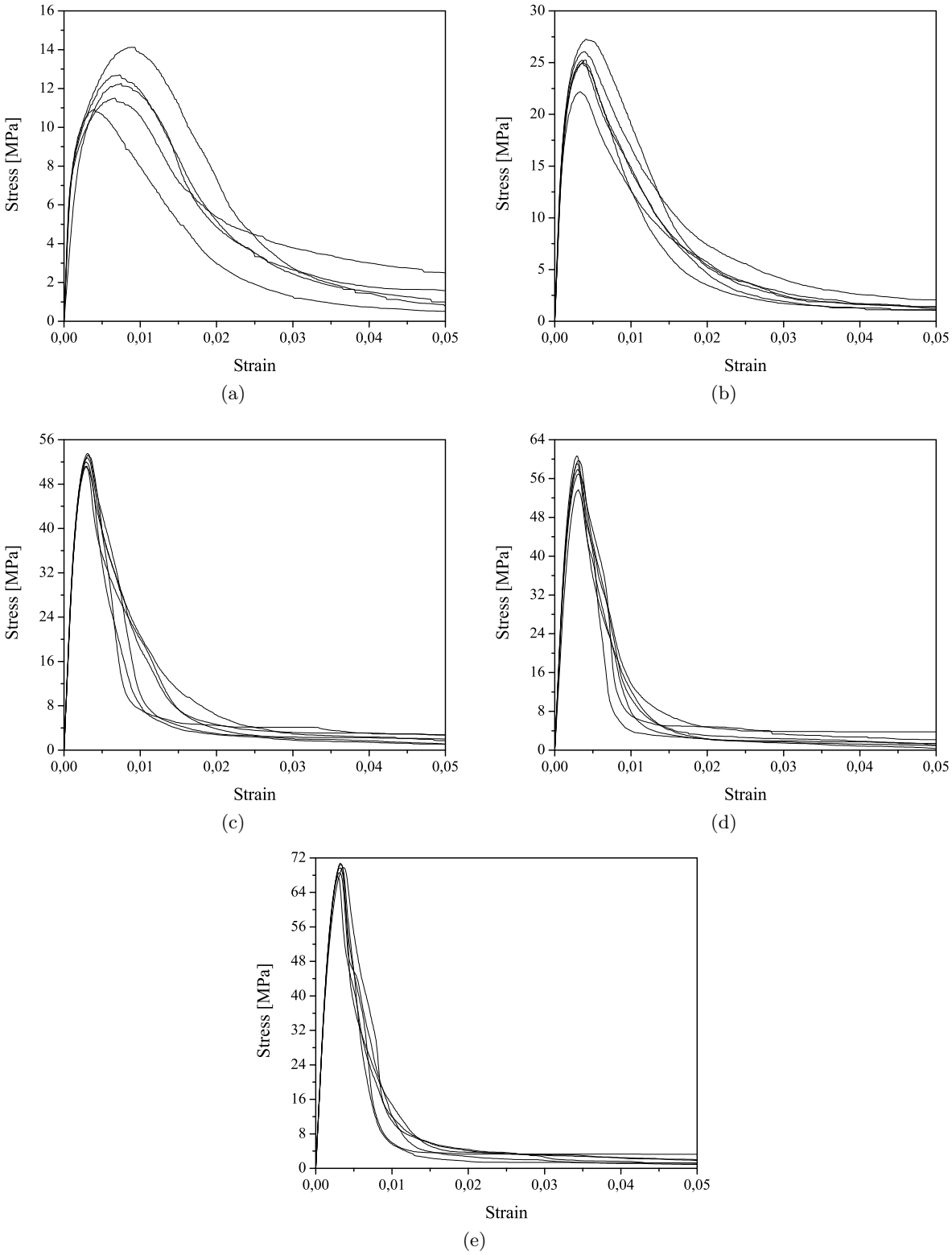

Figure 3.5: Experimental stress-strain relationships for the series *Cf30*: (a) 12 hours, (b) 24 hours, (c) 3 days, (d) 7 days and (e) 28 days.

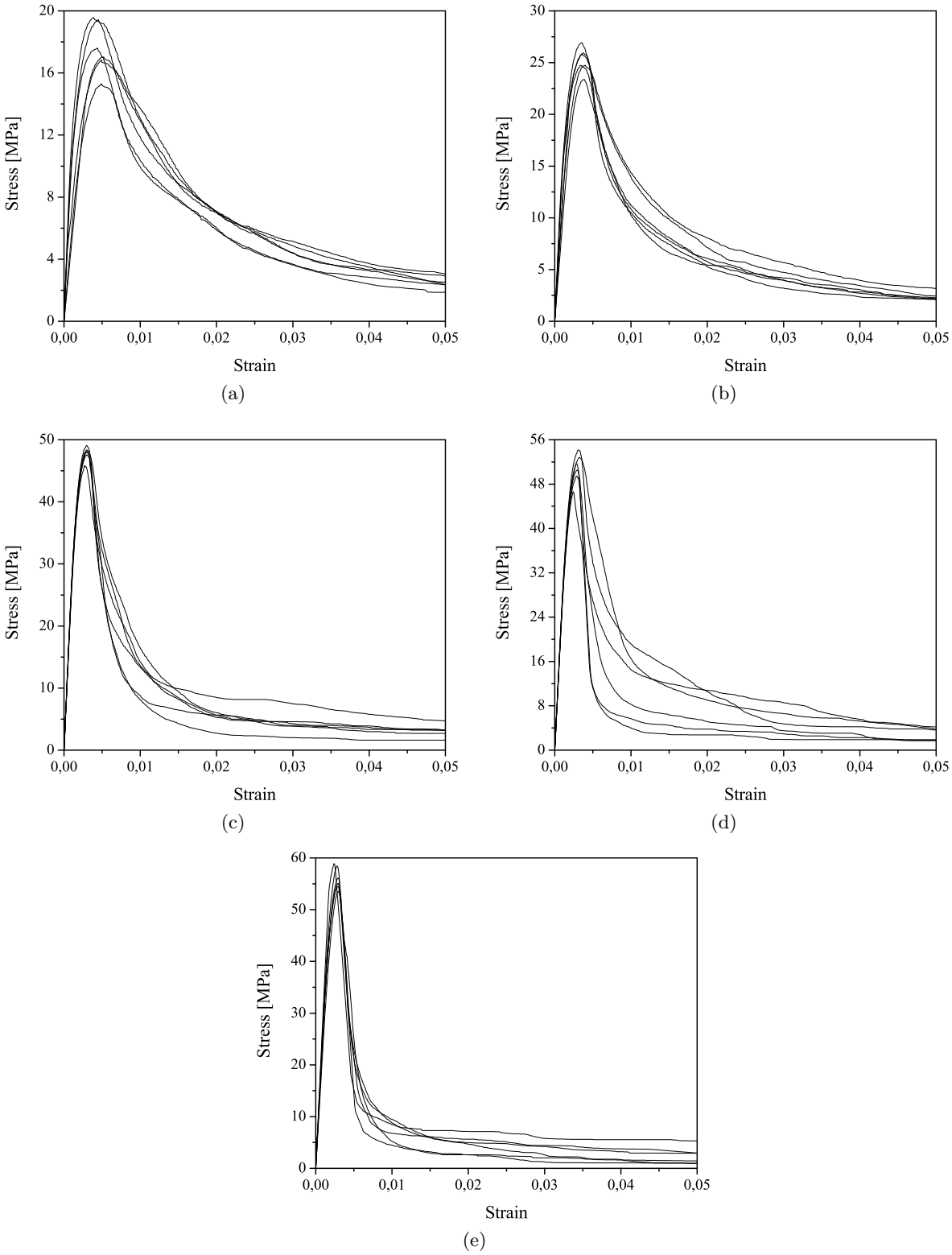

Figure 3.6: Experimental stress-strain relationships for the series *Cf45*: (a) 12 hours, (b) 24 hours, (c) 3 days, (d) 7 days and (e) 28 days.

for the older specimens, 3, 7 and 28 days was higher on the *Cf30* series. For these series, the softening branch was less abrupt than for the series *Cf45*. The residual stress for large deformations was slightly higher in the series *Cf45*.

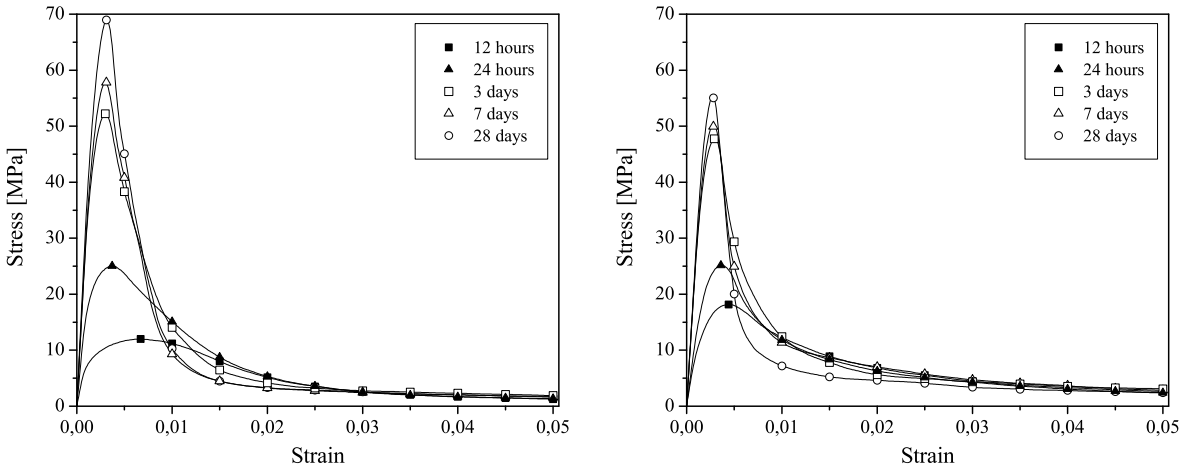

Figure 3.7: Average stress-strain relationships for the series: (a) *Cf30* and (b) *Cf45*.

Since the compressive strength for each series has varied considerably, the $\sigma_c/f_{cm}-\varepsilon$ diagram can better evidence the influence of the fibers on the post-peak behavior for the different series. This diagram for the tested series is represented in Figure 3.8. The more ductile behavior of younger series, 12 and 24 hours, when compared to the older ones is more perceptible from the analysis of these diagrams.

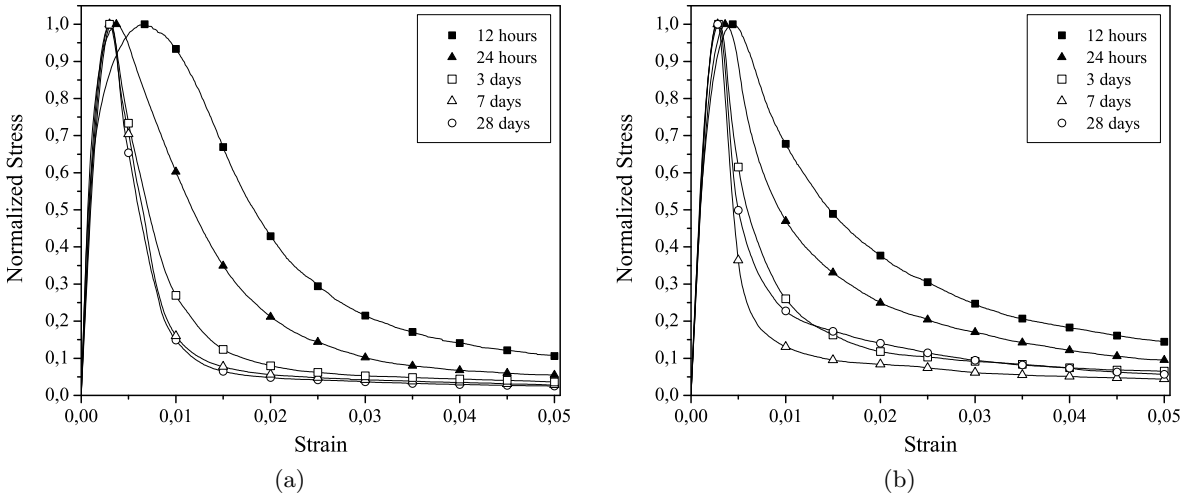

Figure 3.8: Normalized stress-strain relationships for the series: (a) *Cf30* and (b) *Cf45*.

3.3 Age influence on the mechanical properties

3.3.1 Compressive strength

Table 3.2 includes the average values of the compressive strength, f_{cm}, and the correspondent coefficients of variation, CoV. As expected, for both series, the f_{cm} increases with age. At 28 days, the *Cf30* series had a higher compressive strength than the *Cf45* series. The higher content of the binder paste on the series *Cf45* should have lead to higher resistances. In spite of the higher w/c ratio of the *Cf45* series might justify this decrease, more research should be done to understand the influence on the compressive strength of the changes introduced in the solid skeleton from *Cf30* to *Cf45* series.

Table 3.2: Average values of the SFRSCC compressive strength, f_{cm}.

Age	*Cf30*		*Cf45*	
	f_{cm} [MPa]	CoV [%]	f_{cm} [MPa]	CoV [%]
12 h	12.3	9.95	17.6	1.63
24 h	24.7	8.38	25.3	1.24
3 d	52.3	1.90	47.9	1.10
7 d	58.1	4.32	51.0	2.61
28 d	69.7	1.73	56.2	2.15

The influence of age on the concrete compressive strength is depicted in Figure 3.9. The growing process of the f_{cm} has two distinct phases: a high increase up to 3 days and a smooth increase after this age. After 3 days, the f_{cm} increase ratio was even less pronounced for the series *Cf45*.

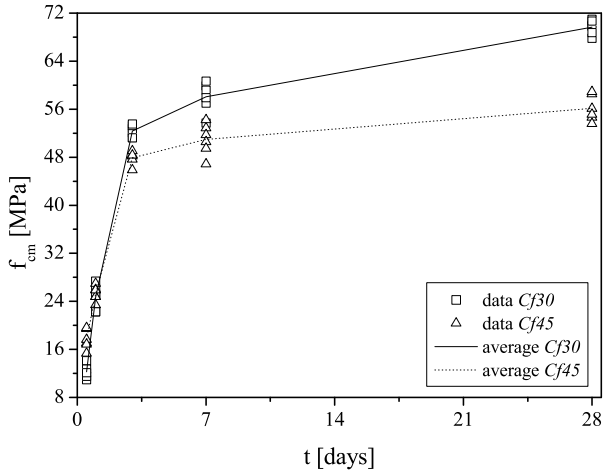

Figure 3.9: Influence of the age on the SFRSCC compressive strength, f_{cm}.

3.3.2 Elasticity modulus

The average values of the elasticity modulus, E_{ci}, and the correspondent coefficients of variation, CoV, are indicated in Table 3.3.

Table 3.3: Average values of the SFRSCC elasticity modulus, E_{ci}.

Age	*Cf30*		*Cf45*	
	E_{ci} [GPa]	CoV [%]	E_{ci} [GPa]	CoV [%]
12 h	13.6	17.86	18.8	7.10
24 h	25.3	4.96	22.4	5.83
3 d	37.1	4.31	31.4	2.04
7 d	40.4	0.78	31.9	2.14
28 d	41.5	2.31	34.5	4.33

The E_{ci} increased with age for both series. The influence of the concrete age on the E_{ci} is depicted in Figure 3.10, from which it can be concluded that E_{ci} has a similar variation with age as f_{cm}. However, for *Cf30* the f_{cm} value increased between 7 and 28 days, while the E_{ci} of the series *Cf30* had a marginal increment in this period. The E_{ci} of the *Cf45* series, after day three, had an increment of only 3 GPa. These results point out that the stiffness of both SFRSCC is almost attained between the age of 3 to 7 days, due to the high matrix capacity of these concretes.

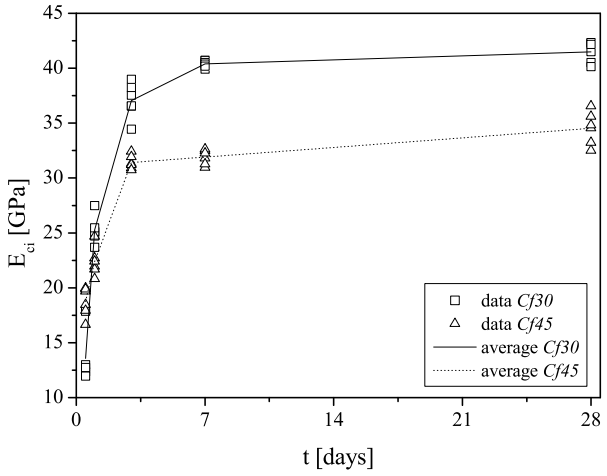

Figure 3.10: Influence of the age on the SFRSCC elasticity modulus, E_{ci}.

3.3.3 Strain at peak stress

The average values of the strain at peak stress, ε_{c1}, and the correspondent coefficients of variation, CoV, are included in Table 3.4. Due to the increase of the concrete stiffness, ε_{c1} decreased with age for both series. Since the increase of E_{ci} after 3 days is not significant, the variation of ε_{c1} is small after this age.

Table 3.4: Average values of the strain at peak stress, ε_{c1}.

Age	*Cf30*		*Cf45*	
	ε_{c1}	CoV [%]	ε_{c1}	CoV [%]
12 h	0.0067	28.90	0.0047	10.25
24 h	0.0039	7.84	0.0037	5.27
3 d	0.0030	3.99	0.0030	5.77
7 d	0.0031	5.14	0.0029	9.55
28 d	0.0031	6.28	0.0028	5.69

Figure 3.11 shows the variation of the ε_{c1} with age. The ε_{c1} decreased abruptly up to 3 days, however after this age the decrease is marginal.

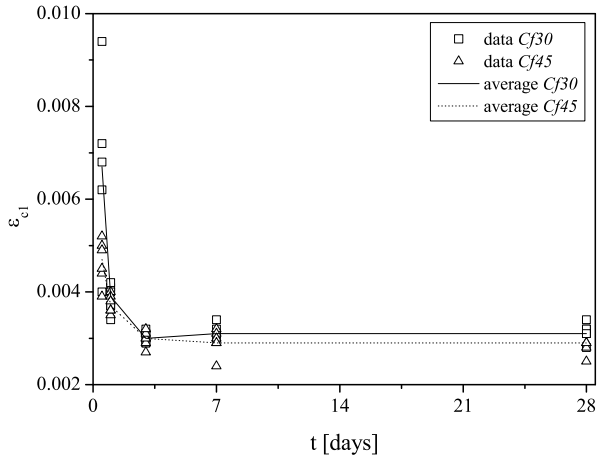

Figure 3.11: Influence of the age on the strain at peak stress, ε_{c1}.

The ε_{c1} values at the age of 28 days obtained for the both series, are approximately about 0.003. Similar values of ε_{c1} were obtained for steel fiber reinforced concrete by L. S. Hsu and C. T. Hsu (1994), Barros (1995), Kooiman (2000) and Cunha (2004). This value is higher than the value of 0.0022, proposed by the CEB – FIP (1993) for plain concrete. On the other hand, the EN 1992-1-1 (2004) suggests different values of ε_{c1} for the distinct concrete strength classes.

For the average compressive strength of the *Cf30* series, the value suggested by this standard is 0.0026, whereas for the average strength of *Cf45* series the value proposed is 0.00245. This difference is due to the effect of the fibers bridging the cracks that are formed just before the peak load.

3.3.4 Energy dissipated under compression

The energy dissipated per unit volume under compression, G_c, was calculated as the area under the stress-strain curve, $\sigma_c - \varepsilon_c$. This value can be computed using Equation 3.1. The G_c value was always determined until a ultimate deformation, ε_u, of 0.05, where it was expected that the residual strength would be small.

$$G_c = \int_0^{\varepsilon_u} \sigma_c \, d\varepsilon \tag{3.1}$$

Table 3.5 includes the average values of G_c and the corresponding coefficients of variation, CoV. In general, the concrete energy absorption increased with age. The values of the coefficients of variation however, are quite high. The major part of the energy is released in the softening phase that is too dependent on the fiber reinforcement mechanisms provided by fibers crossing the cracks. The efficiency of those mechanisms depend considerably on the fiber bond length and fiber orientation towards the cracks they bridge, whose homogeneity can not be assumed between two, apparently, equal batches. This justifies the high CoVvalues attained for the G_c.

Table 3.5: Average values of the energy dissipated under compression.

Age	*Cf30*		*Cf45*	
	G_c [N/mm^2]	CoV [%]	G_c [N/mm^2]	CoV [%]
12 h	0.26	18.03	0.33	12.35
24 h	0.36	13.13	0.38	12.01
3 d	0.48	12.70	0.46	19.73
7 d	0.44	14.84	0.47	34.37
28 d	0.49	10.31	0.39	18.77

The influence of the age on the G_c values is represented in Figure 3.12. The G_c had an abrupt increase up to the 3 days, and kept almost constant after this age. The observed decrease on the G_c, for the series *Cf30* with 7 days, and in the series *Cf45* with 28 days is justified with the smaller number of fibers on the rupture surface, as referred in the section 3.1.

The variation of the energy dissipated under compression, G_c, with the strain is represented in Figure 3.13. In general, G_c increased with strain more swiftly for the older specimens, 3, 7

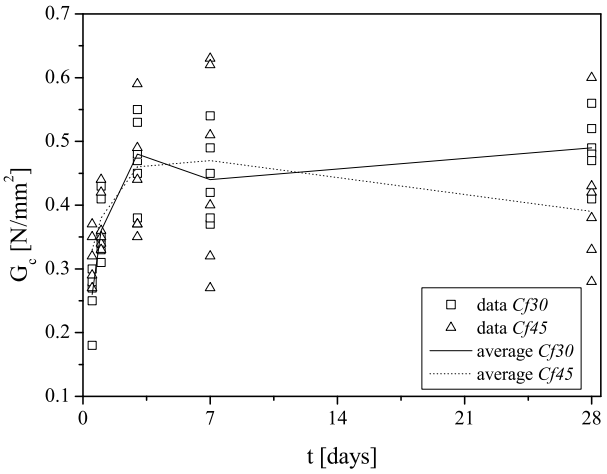

Figure 3.12: Energy dissipated under compression, G_c.

and 28 days than for the specimens with 12 and 24 hours. The only exception was for the series *Cf30* with 7 days. For the latter series was observed a smaller number of fibers on the fracture surface, which justifies the lower G_c value.

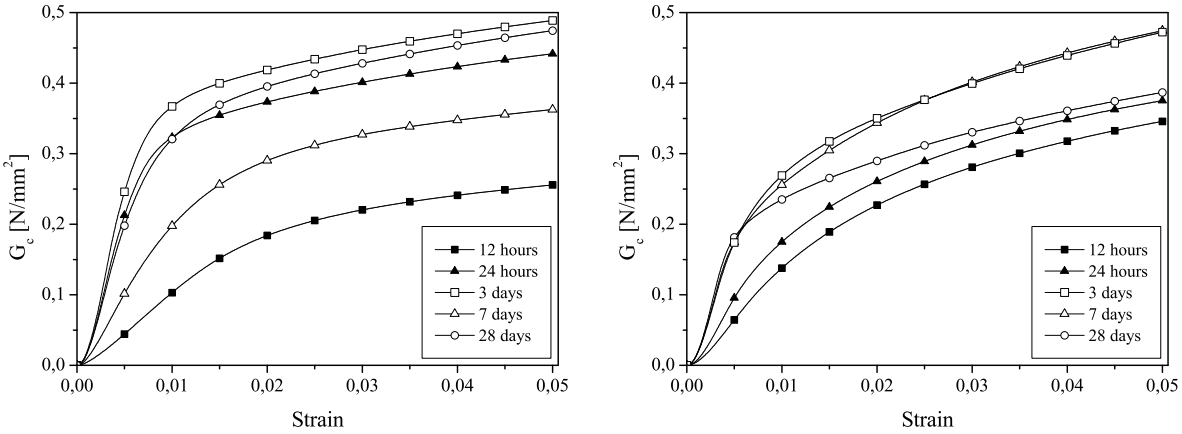

(a) (b)

Figure 3.13: Relationship between G_c and strain: (a) *Cf30* and (b) *Cf45*

3.4 Compressive toughness index

The concrete toughness represents the material ability to absorb energy. A convenient way to quantify the increase of toughness provided by the fiber reinforcement is to define a toughness index, T.I., which is the ratio between the energy dissipated by the fiber reinforced concrete, up to a given strain limit, and the energy dissipated by its correspondent plain concrete (L. S.

Hsu and C. T. Hsu, 1994). The toughness was computed using Equation 3.1, until to levels of strain, 0.001 and 0.005. The stress-strain relationship for the plain concrete proposed by the CEB – FIP (1993) was used to determine the toughness of this concrete. In order to define the stress-strain relationship, the values of f_{cm}, E_c must be known. For this purpose the values of Tables 3.2, 3.3 were used for each series of the steel fiber concrete. The ε_{c1} value for the plain concrete was always 0.0022.

In Figure 3.14 is represented the variation of the parameter T.I. with the reinforcement index, $R.I. = V_f \times l_f/d_f$, where V_f, l_f and d_f are, respectively, the fiber volume content, the fiber length and the fiber diameter. Notice that l_f/d_f is the fiber aspect ratio.

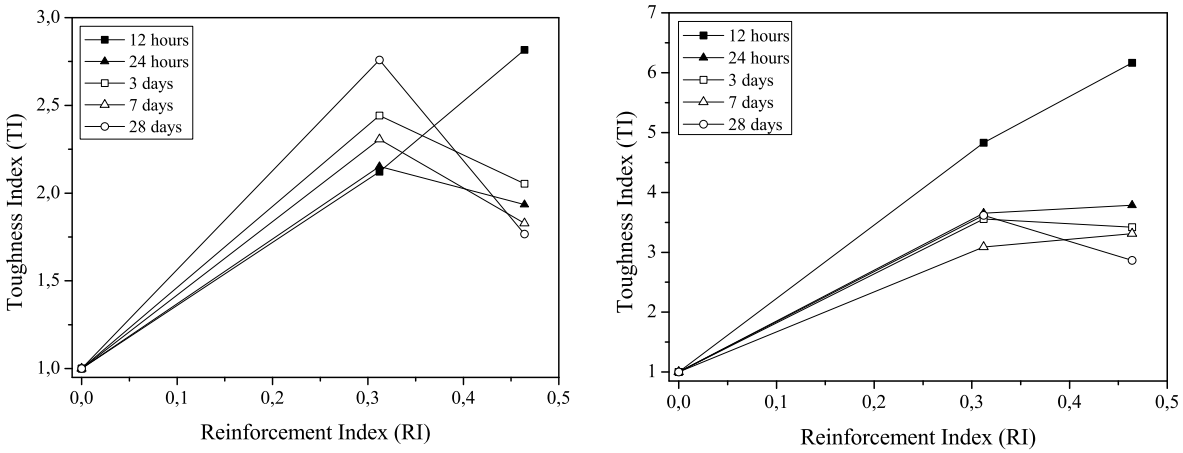

Figure 3.14: Variation of the toughness index with the reinforcement index up to a strain of: (a) 0.01 and (b) 0.05.

Figure 3.14(a) shows the T.I., calculated until a deformation of 0.01. The value of T.I. for the *Cf30* series ($R.I = 0.33$), is in the range $[2, 2.75]$, meaning that the energy absorption of this concrete is 2 to 2.75 times higher that the one absorbed by the correspondent plain concrete, until a deformation of 0.01. On the other hand, for *Cf45* series ($R.I. = 0.47$), apart series of 12 hours, the values of T.I. have decreased comparatively to the ones of *Cf30* series. This suggests that, for the designed SFRSCC, up to a deformation of 0.01, the increment of fiber content was not efficient in what concerns to its energy absorption capability. As already it was pointed out, this effect might be justified by the evolution of compressive strength and elasticity modulus of the SFRSCC of the *Cf30* and *Cf45* series.

In Figure 3.14(b) the T.I. was calculated until a deformation of 0.05. The values of T.I when compared to those obtained until a deformation of 0.01, increased substantially. The toughness index, for deformations up to 0.05, increased with the reinforcement index. The only exception

was the series with 28 days, that can be justified by the larger difference of the f_{cm} and E_{ci} between *Cf30* and *Cf45* series, for this age.

Chapter 4

Expressions for the analytical simulation

4.1 Statistic control

The experimental data presented in the previous chapter will be used to obtain expressions for evaluating the influence of age on the properties of the designed SFRSCC. In this section it will be presented the statistical treatment done to the experimental data. From the sample distribution, and adopting a confidence interval, $100(1-\alpha)$, of 95%, the lower and upper-confidence limits were determined. All the values from the samples that were not inside this confidence interval, were disregarded to determine the expressions for evaluating the influence of age on the properties of SFRSCC. The confidence intervals were determined by the following expression (Montgomery and Runger, 1994):

$$\bar{x} - z_{\alpha/2}\ \sigma/\sqrt{n} \leq \mu \leq \bar{x} + z_{\alpha/2}\ \sigma/\sqrt{n} \tag{4.1}$$

where n is the number of sample values, $\bar{x}$ and μ are, respectively, the mean of the sample and the mean of the population; σ^2 and $z_{\alpha/2}$ are, respectively, the variance and the upper $\alpha/2$ percentage point of the standard normal distribution. For small samples from non-normal populations the confidence level may not be exact. The lower and upper-confidence limits obtained for the experimental data samples are presented on Annex II.

4.2 Fitting method

To obtain expressions for the evaluation of the age influence on the concrete compressive strength, elasticity modulus, strain at peak-stress and energy absorption capacity, the non-linear square method was used (Ryan, 1997). This method was also applied to obtain a time-dependent function defining a parameter used on the evaluation of the $\sigma(t) - \varepsilon(t)$ relationships for the defined SFRSCC. On any fitting procedure there are two main blocks:

1. The data obtained experimentally as a result of some measurements, in which one or several independent variables $(x_{i1}, x_{i2}, \ldots)$, e.g. *strain*, are varied over a certain range, in a controllable manner, so as to produce the measured dependent variable(s) $(y_{i1}, y_{i2}, \ldots)$, e.g. *stress*.

2. The mathematical expression, $y_i = f_i(x_{i1}, x_{i2}, \ldots; p_{k1}, p_{k2}, \ldots)$, that represents the theoretical model used to reproduce the experimental data. The model usually depends on one or more parameters $(p_{k1}, p_{k2}, \ldots)$.

The aim of the fitting procedure is to find the values of the parameters which best describe the data. The best fitting was defined by choosing the parameters so that the sum of the squares of the deviations of the theoretical curve from the experimental points, for a range of independent variables, is minimum (see Equation 4.2).

$$\chi^2(p_{k1}, p_{k2}, \ldots) = \frac{1}{n^{eff} - p} \sum_i \sum_j w_{ij} \Big[y_{ji} - f_j(x_{i1}, x_{i2}, \ldots; p_{k1}, p_{k2}, \ldots) \Big]^2 \tag{4.2}$$

where, y_{ji} are the measured values of the dependent variable, y_j, for the values of the independent variables, n^{eff} is the total number of experimental points used in the fitting, and p is the total number of adjustable parameters used in the fitting (the difference $d = n^{eff} - p$ is usually referred to as the number of degrees of freedom). The quantities w_{ij} represent the weights of each experimental point. In the present case there was no weighting therefore w_{ij}=1.

The minimization of $\chi^2(p_{j1}, p_{j2}, \ldots)$ is performed by a series of iterations on the parameter values and computing Equation 4.2 at each stage. In order to accomplish that, the partial derivates $f_j' = [\partial f_j/\partial p_{k1},\ \partial f_j/\partial p_{k2}, \ldots,\ \partial f_j/\partial p_{kp}]$ are determined for the parameters at each iteration.

4.3 Analytical expressions for the mechanical properties

In this section, the fitting method is applied for the establishment of analytical expressions to predict the most significant properties of the self-compacting steel fiber reinforced concrete,

SFRSCC, at an age t: compressive strength, f_{cm}, the elasticity modulus, E_{ci}, strain at peak stress, ε_{c1} and the energy dissipated under compression, G_c.

4.3.1 Compressive strength, f_{cm}

To estimate the compressive strength of plain concrete at various ages, $f_{cm}(t)$, the CEB – FIP (1993) suggests an expression similar to the subsequent one:

$$f_{cm}(t) = f_{cm,28} \cdot \exp\left\{a\left[1 - \left(\frac{28}{t}\right)^{b}\right]\right\} \tag{4.3}$$

where $f_{cm,28}$ is the mean compressive strength value at 28 days, and a, b are two dimensionless parameters. For plain concrete, CEB – FIP (1993) proposes $a = 0.2$, in case of using rapid hardening high strength cements, and a constant value of 0.5 for parameter b.

Using the $f_{cm,28}$ values obtained in the tested SFRSCC series, the $f_{cm}(t)/f_{cm,28}$ function, evaluated according to the CEB – FIP (1993) proposal, is depicted in Figure 4.1. In spite of the fact that the obtained correlation factors, R^2, were quite high, the compressive strength predicted by Equation 4.3 at the ages of 3 and 7 days was underestimated, particularly, for the series with 45 kg/m^3 of steel fibers.

Using the fitting procedure described in the previous section, the values of parameters a and b of Equation 4.3 were determined in order to improve its capability of simulating the age effect on the developed SFRSCC compressive strength. The degree of the simulation of the fitted curve increased considerably, specially at the ages of 3 and 7 days. The values of the fitted curve parameters, as well as, the values of R^2 are included in Figure 4.1.

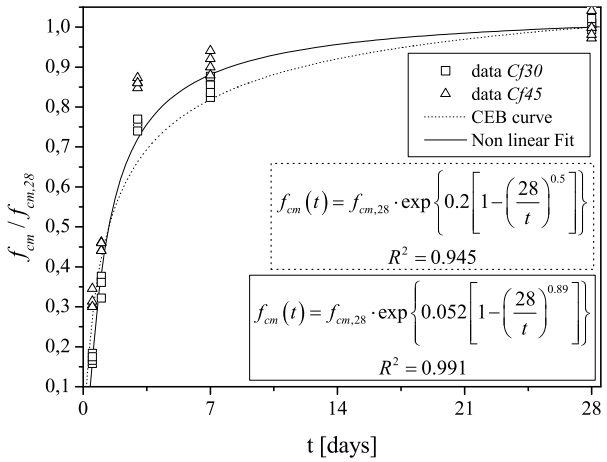

Figure 4.1: Simulation of the age influence on the concrete compressive strength.

4.3.2 Elasticity modulus, E_{ci}

In resemblance to the compressive strength, CEB – FIP (1993) proposes the following expression:

$$E_{ci}(t) = E_{ci,28} \cdot \left\{ \exp\left\{ a \left[1 - \left(\frac{28}{t} \right)^{b} \right] \right\} \right\}^{c} \tag{4.4}$$

to determine the elasticity modulus at an age of t days, $E_{ci}(t)$, where $E_{ci,28}$ is the elasticity modulus at an age of 28 days, a, b and c are dimensionless parameters. The CEB – FIP (1993) indicates for plain concrete $c = 0.5$, whereas the values of a and b are the same ones as those proposed for the Equation 4.3.

Using the $E_{ci,28}$ values obtained in the tested SFRSCC series, the $E_{ci}(t)/E_{ci,28}$ function, evaluated according to the CEB – FIP (1993) recommendation, is depicted in Figure 4.2. The CEB – FIP (1993) approach underestimates the elastic modulus at the ages of 3 and 7 days, and overestimates it at the age of 12 hours.

Fitting the parameters a, b and c of Equation 4.4, the accuracy of the fitted curve increased considerably. The fitted curve parameters, as well as the values of R^2 are indicated in Figure 4.2.

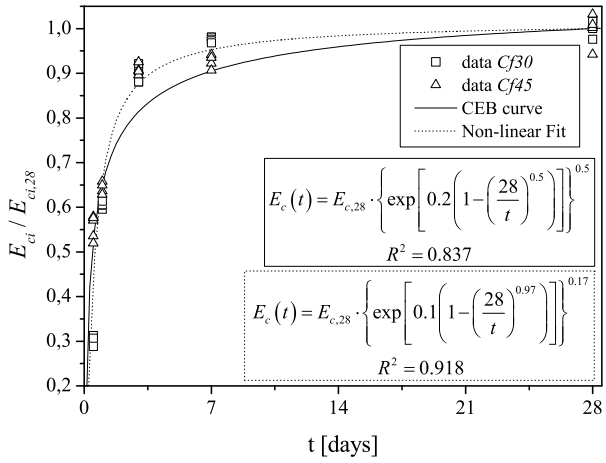

Figure 4.2: Simulation of the age influence on the concrete elasticity modulus.

The CEB – FIP (1993) also proposes Equation 4.5 for determining the relationship between the elasticity modulus, E_{ci}, and the average compressive strength, f_{cm}, in which, for plain concrete, $E_{c0} = 21.5$ GPa, $f_{cm0} = 10$ MPa and $a = 1/3$.

$$E_{ci} = E_{c0} \cdot \left(\frac{f_{cm}}{f_{cm0}} \right)^{a} \tag{4.5}$$

The relationship between the elasticity modulus and the compressive strength is depicted in Figure 4.3. This figure also includes the analytical expression suggested by CEB – FIP (1993) and the one obtained by the non linear fitting procedure. Fitting parameters E_{c0} and a increased substantially the adjustment of Equation 4.5 to the experimental data and consequently the correlation factor.

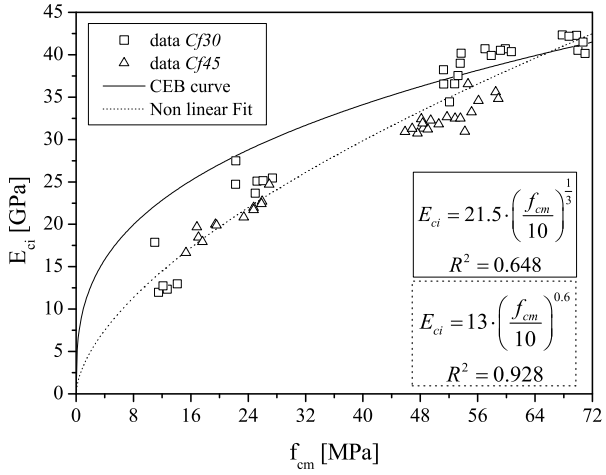

Figure 4.3: Analytical relationships between the elasticity modulus and the compressive strength.

4.3.3 Strain at peak stress, ε_{c1}

For predicting the influence of concrete age on the strain at peak stress, $\varepsilon_{c1}(t)$, it was used an hyperbolic function indicated in Equation 4.6, where $\varepsilon_{c1,28}$ is the strain at peak stress for the age 28 days. This expression was adjusted to the experimental data by fitting the dimensionless parameter a.

$$\varepsilon_{c1}(t) = \frac{\varepsilon_{c1,28} \cdot \dfrac{t}{28}}{a + \dfrac{t}{28}} \tag{4.6}$$

The analytical relationship obtained by applying the fitting procedure to Equation 4.6 is represented in Figure 4.4. The quality of the adjustment of the previous equation is quite good, however the obtained correlation factor is not too high. This is mainly due to the high scatter of the strain at peak stress observed for the age of 12 hours.

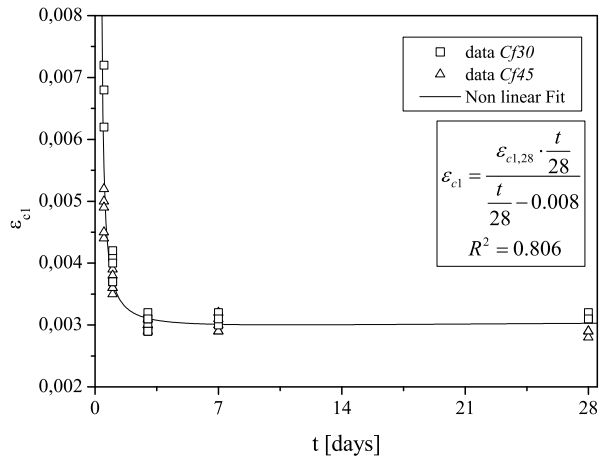

Figure 4.4: Simulation of the age influence on the strain at peak-stress, ε_{c1}.

4.3.4 Energy dissipated under compression, G_c

For the two tested series, the variance of the energy dissipated under compression, in respect to age, was distinct. To attain the relationship between the energy dissipated and age, $G_c(t)$, it was used Equation 4.7. In both series was observed a high scatter of G_c, especially in the *Cf45* series.

$$G_c(t) = \frac{a \cdot \frac{t}{28}}{b + \frac{t}{28}} + \frac{c}{d + \frac{t}{28}} + e \cdot \frac{t}{28} \tag{4.7}$$

The variation of G_c with time, for both series, is depicted in Figure 4.5. The values of the parameters a, b, c, d and e obtained in the fitting procedure are indicated on Equation 4.8. The correlation factor was small, $R^2 = 0.589$, due to the high scatter observed.

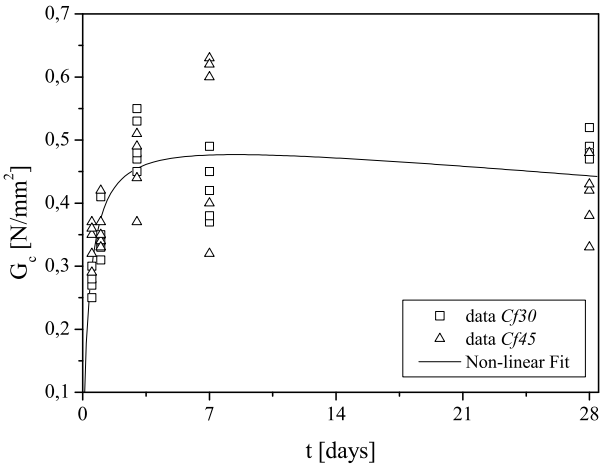

Figure 4.5: Simulation of the age influence on the energy dissipated under compression.

$$G_c(t) = \frac{0.52 \cdot \frac{t}{28}}{0.013 + \frac{t}{28}} + \frac{0.00011}{0.18 + \frac{t}{28}} - 0.07 \cdot \frac{t}{28} \tag{4.8}$$

4.4 Analytical stress-strain relationships

The $\sigma_c - \varepsilon_c$ relationships available for modeling the compressive behavior of plain (Carreira and Chu, 1985; CEB – FIP, 1993) and fiber reinforced concrete (Ezeldin and Balaguru, 1992; L. S. Hsu and C. T. Hsu, 1994) cannot be directly applied to the developed SFRSCC since the fitting degree they provide is not good enough. Therefore a new approach is proposed, in this section, to obtain a $\sigma_c - \varepsilon_c$ analytical expression that can predict the compression behavior registered in the tested SFRSCC.

The expression adopted in the present work is similar to the one proposed by the CEB – FIP (1993) for plain concrete. The stress – strain diagram for loading under compression is represented schematically in Figure 4.6. In fact, the equation that corresponds to the branch represented by a straight line in Figure 4.6 is the same one proposed by the CEB – FIP (1993). For this branch, the stress – strain relationship is given by the following function:

$$\sigma(\varepsilon_c) = \frac{\frac{E_{ci}}{E_{c1}} \cdot \frac{\varepsilon_c}{\varepsilon_{c1}} - \left(\frac{\varepsilon_c}{\varepsilon_{c1}}\right)^2}{1 + \left(\frac{E_{ci}}{E_{c1}} - 2\right) \cdot \frac{\varepsilon_c}{\varepsilon_{c1}}} \cdot f_{cm} \qquad \text{for } \varepsilon_c \leq \varepsilon_{c,lim} \tag{4.9}$$

where E_{ci} and E_{c1} are, respectively, the tangent modulus and the secant modulus from the origin to the peak compressive stress ($E_{c1} = f_{cm}/\varepsilon_{c1}$); σ_c, ε_c and ε_{c1} are the compression stress (MPa), the compression strain and the strain at the peak compressive stress, respectively. The strain $\varepsilon_{c,lim}$ limits the applicability of Equation 4.9 (see Figure 4.6).

For the descending part of the stress – strain diagram, Equation 4.9 is valid only for strain values up to $\varepsilon_{c,lim}$. The strain $\varepsilon_{c,lim}$ at $\sigma_{c,lim}$ ($= \alpha \cdot f_{cm}$) may be computed from Equation 4.10.

$$\varepsilon_{c,lim} = \left[\frac{1}{2}\left[(1-\alpha)\cdot\frac{E_{ci}}{E_{c1}} + 2\,\alpha\right] + \left[\frac{1}{4}\left[(1-\alpha)\cdot\frac{E_{ci}}{E_{c1}} + 2\,\alpha\right]^2 - \alpha\right]^{0.5}\right]\varepsilon_{c1} \tag{4.10}$$

For $\varepsilon_c > \varepsilon_{c,lim}$ the descending branch of the $\sigma_c - \varepsilon_c$ diagram (dashed line in Figure 4.6) is described using an equation of the type:

$$\sigma(\varepsilon_c) = \left[a\left(\frac{\varepsilon_c}{\varepsilon_{c1}}\right)^2 + b\,\frac{\varepsilon_c}{\varepsilon_{c1}}\right]^{-1} \cdot f_{cm} \qquad \text{for } \varepsilon_c > \varepsilon_{c,lim} \tag{4.11}$$

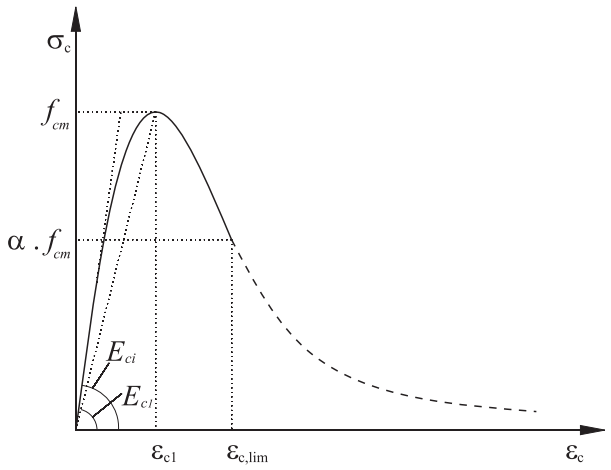

Figure 4.6: Stress strain diagram for uniaxial compression (CEB – FIP, 1993).

where the values of parameters a and b are determined in order to assure the continuity of the function at the point $\varepsilon_{c,lim}$. Since the following conditions should be assured:

$$\begin{cases} \underbrace{\sigma_c(\varepsilon_{c,lim})}_{\text{equation 4.9}} = \underbrace{\sigma_c(\varepsilon_{c,lim})}_{\text{equation 4.11}} \\ \underbrace{\left.\dfrac{\partial \sigma_c}{\partial \varepsilon_c}\right|_{\varepsilon_{c,lim}}}_{\text{equation 4.9}} = \underbrace{\left.\dfrac{\partial \sigma_c}{\partial \varepsilon_c}\right|_{\varepsilon_{c,lim}}}_{\text{equation 4.11}} \end{cases} \tag{4.12}$$

Equation 4.11 is converted into the following one:

$$\sigma(\varepsilon_c) = \left[\left[\frac{1}{\dfrac{\varepsilon_{c,lim}}{\varepsilon_{c1}}} \xi \cdot \left(\frac{1}{2\,\alpha}\right)^2 - \frac{1}{\left(\dfrac{\varepsilon_c}{\varepsilon_{c1}}\right)^2} \cdot \frac{1}{\alpha} \right] \left(\frac{\varepsilon_c}{\varepsilon_{c1}}\right)^2 + \left[\frac{1}{\dfrac{\varepsilon_{c,lim}}{\varepsilon_{c1}}} \cdot \frac{2}{\alpha} - \xi \left(\frac{1}{2\,\alpha}\right)^2 \right] \frac{\varepsilon_c}{\varepsilon_{c1}} \right]^{-1} \cdot f_{cm} \tag{4.13}$$

with

$$\xi = \frac{4 \left[\left(\dfrac{\varepsilon_{c,lim}}{\varepsilon_{c1}}\right)^2 \left(\dfrac{E_{ci}}{E_{c1}} - 2\right) + 2\,\dfrac{\varepsilon_c}{\varepsilon_{c1}} - \dfrac{E_{ci}}{E_{c1}} \right]}{\left[\dfrac{\varepsilon_{c,lim}}{\varepsilon_{c1}} \left(\dfrac{E_{ci}}{E_{c1}} - 2\right) + 1 \right]^2} \tag{4.14}$$

If $\alpha = 0.5$, Equations 4.10 and 4.13 become those proposed by the CEB – FIP (1993).

In order to evaluate the applicability of the previous described relationship in the present experimental research, the following assumptions were done: the values of the elastic modulus, compressive strength and strain at peak-stress, used in the simulation, were those obtained experimentally for each series; the parameter α was adjusted in order to obtain the best fit of the analytical expression to the average stress-strain curve recorded experimentally.

The analytical stress-strain curves obtained from the best fit procedure and the experimental envelope are depicted in Figures 4.7 and 4.8. The accuracy of the proposed expression toward the experimental data is quite high.

The pre-peak phase was well simulated with the law suggested by CEB – FIP (1993), just by using the values of f_{cm}, E_{ci} and ε_{c1} obtained experimentally for the SFRSCC. For the series with 30 kg/m^3 of fibers, the post-peak behavior was also modeled with exactness until high deformations. For this content of fibers, at the ages of 7 and 28 days (see Figures 4.7(d) and 4.7(e)) the residual strength was slightly underestimated after strains higher than 0.04. On the other hand, for the series with a content of 45 kg/m^3 of fibers, at the age of 12 and 24 hours, the first part of the descending branch correspondent to the analytical curve is slightly less sharp than the experimental envelope. For the 28 day series, the post-peak behavior is only correctly simulated up to a strain of 0.01. After this strain level the residual strength is underestimated (see Figure 4.8(e)).

The Table 4.1 includes the values of the parameter α obtained in the non-linear fitting procedure. The α parameter increased with age and tend to the limit value of 0.9.

Table 4.1: Values of parameter α obtained on the non linear fitting procedure.

Age	12 h	24 h	3 d	7 d	28 d
Cf30	0.423	0.657	0.839	0.871	0.889
Cf45	0.675	0.776	0.876	0.890	0.860

In Figure 4.9 is presented an exponential function used to estimate the evolution of the parameter α with age. Additionally, the value suggested by CEB – FIP (1993) for plain concrete is represented. The values of α obtained on the fitting procedure for the developed SFRSCC are higher than the value proposed for plain concrete, excluding the series *Cf30* at 12 hours. Equation 4.15 simulates the variation of parameter α with age. The correlation factor (R^2) obtained was 0.797.

$$\alpha(t) = 0.9 \cdot \exp\left\{0.005\left[1 - \left(\frac{28}{t}\right)^{1.16}\right]\right\} \tag{4.15}$$

Due to the distinct compressive strengths for the series *Cf30* and *Cf45* at the same age, and

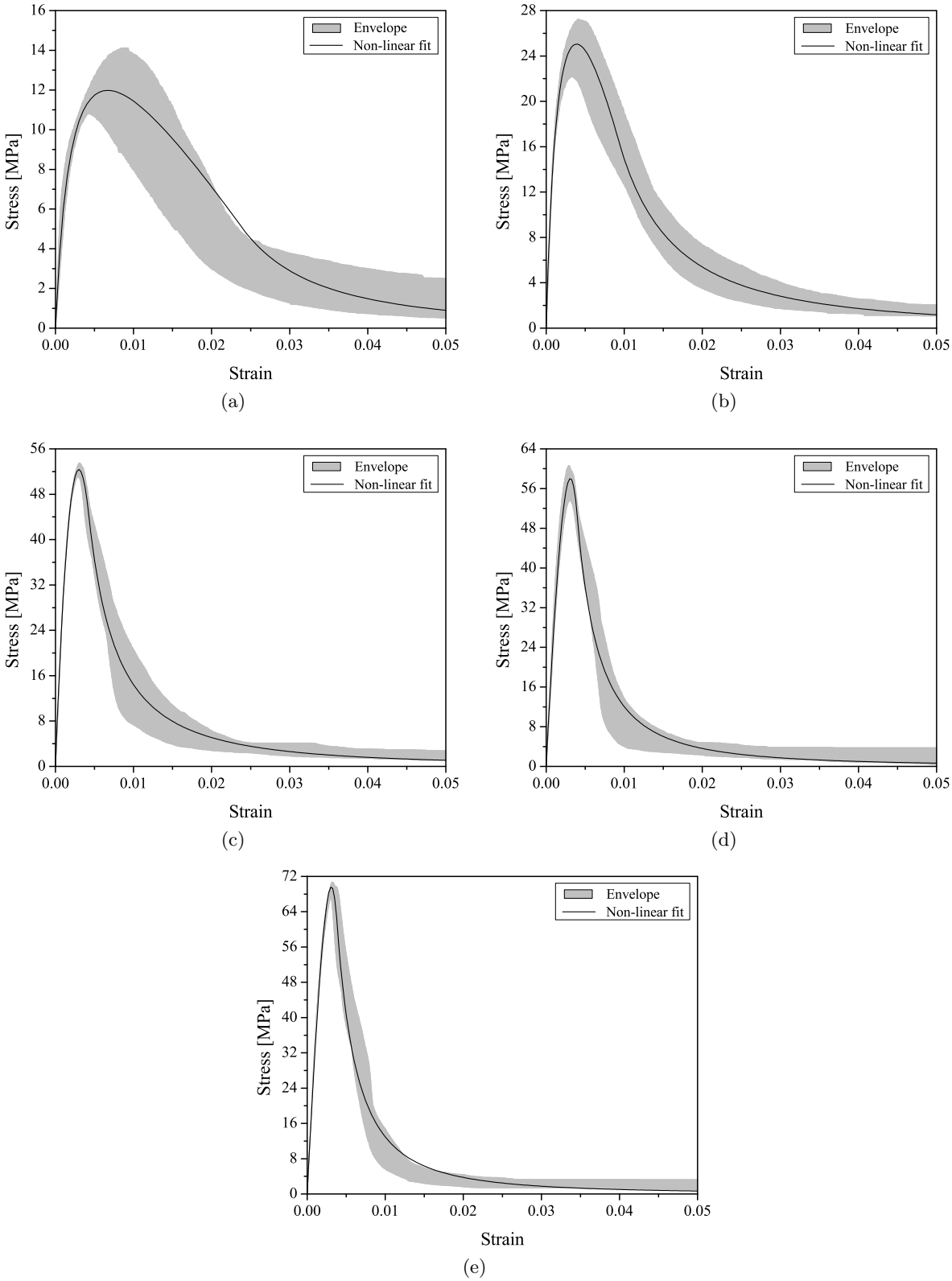

Figure 4.7: Experimental and analytical stress-strain relationships for the *Cf30* series: (a) 12 hours, (b) 24 hours, (c) 3 days, (d) 7 days and (e) 28 days.

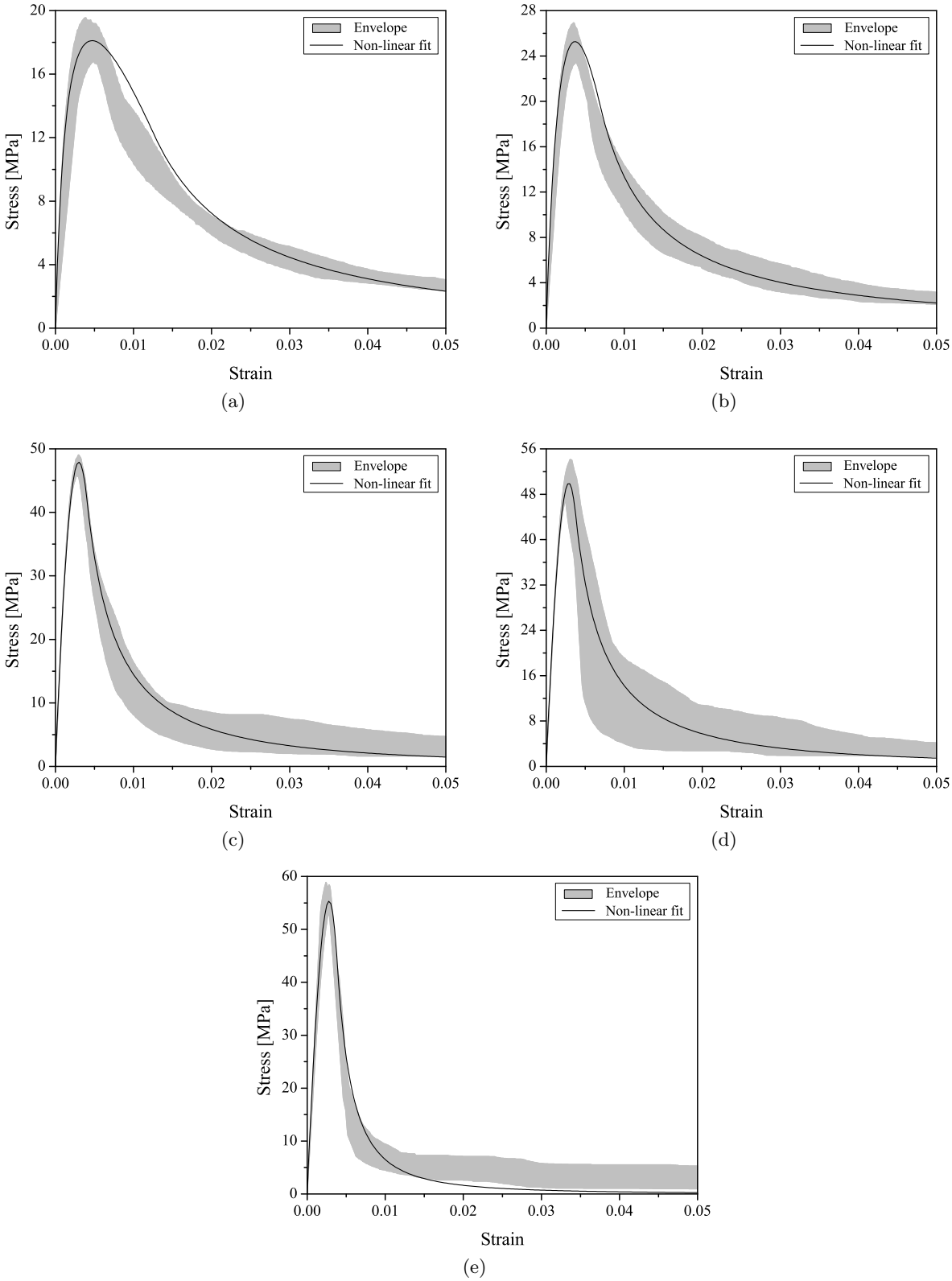

Figure 4.8: Experimental and analytical stress-strain relationships for the *Cf45* series: (a) 12 hours, (b) 24 hours, (c) 3 days, (d) 7 days and (e) 28 days.

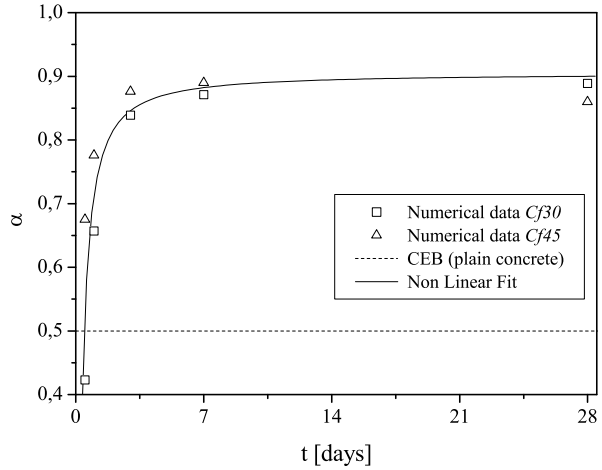

Figure 4.9: Relationship between parameter α and age.

considering that the compressive strength influences significantly the shape of stress - strain curve, better results are attained relating the parameter α with the compressive strength.

In Figure 4.10 is presented the exponential function (see Equation 4.16) used to estimate the evolution of the parameter α with the compressive strength. The degree of accuracy increased significantly. The value of correlation factor was 0.938.

$$\alpha(f_{cm}(t)) = 0.87 \cdot \exp\left\{0.04\left[1 - \left(\frac{f_{cm,28}}{f_{cm}(t)}\right)^{1.8}\right]\right\} \tag{4.16}$$

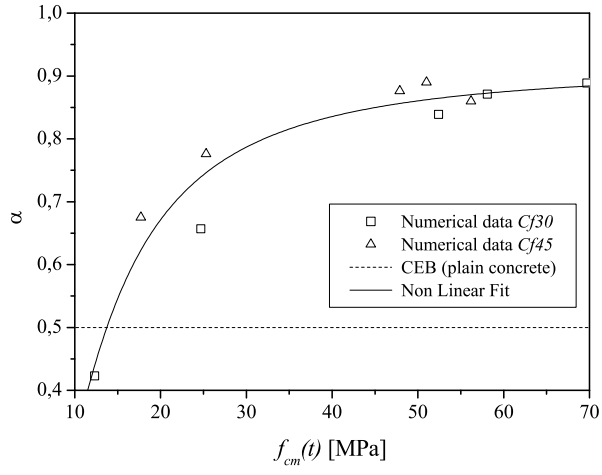

Figure 4.10: Relationship between parameter α and the compressive strength.

Chapter 5

Conclusions

5.1 Conclusions

An experimental programme was carried out to evaluate the influence of the fiber content and concrete age on the compressive behavior of steel fiber reinforced self-compacting concrete, SFRSCC.

The main mechanical properties of the SFRSCC, such as: the compressive strength, f_{cm}, the elasticity modulus, E_{ci}, strain at peak stress, $\varepsilon_{c,1}$ and the volumetric energy dissipated, G_c, were assessed for the ages of 12 hours, 24 hours, 3, 7 and 28 days. Two distinct contents of fibers were considered, 30 kg/m^3 and 45 kg/m^3.

The compressive strength, as well as the elasticity modulus increased with age, mainly in the recent ages, i.e. until the 3 days. Increasing the fiber content from 30 kg/m^3 to 45 kg/m^3, in general, a decrease of f_{cm} and E_{ci} values was observed. This might be justified by the increase of the water/cement ratio and percentage of limestone filler, as well as the changes introduced in the solid skeleton from *Cf30* to *Cf45* series. More research in this field should be done to get more clear evidences of these aspects.

The strain at peak stress decreased with age for both series of distinct contents of fibers. The value obtained experimentally, for the 28 days, was slightly higher than the one of the corresponding plain concrete, and is similar to the values obtained by several authors for steel fiber reinforced concrete. In general, the energy dissipated under compression, G_c increased with age. However, it was not observed a significant change with the increment of the fiber content, form 30 kg/m^3 to 45 kg/m^3. Some series presented a lower value of G_c than it was expected. This can be justified with the number of fibers found on the rupture surface of these specimens. For the series of 3, 7 and 28 days the failure mode was exclusively by shear, whereas in the younger specimens two more types of failure modes were observed.

Analytical expressions to predict the most significant mechanical properties of the developed

SFRSCC at an age t were presented. A stress-strain relationship was proposed to model the behavior of the SFRSCC since the early ages. This relation was capable of modeling the complete compressive behavior of SFRSCC with a high accuracy.

Chapter 6

References

ACI 544.1R. "State-of-the-art report on fiber reinforced concrete." Technical report, American Concrete Institute (1997).

ACI Committee 544. "Measurement of properties of fiber reinforced concrete." *ACI Materials Journal*, 583–593 (1988).

ASTM C469. "Standard test method for static modulus of elasticity and poisson's ratio of concrete in compression." *Annual Book of ASTM Standards, American Society of Testing Materials*, 4(2): 241–244 (1994).

Balaguru, P. N. and Shah, S. P. *Fiber Reinforced Cement Composites*. McGraw-Hill Inc, New York (1992).

Barros, J. A. O. *Comportamento do betão reforçado com fibras, análise experimental e simulação numérica*. Ph.D. thesis, Faculdade de Engenharia da Universidade do Porto, Portugal (in Portuguese) (1995).

Camões, A. F. F. *Betões de elevado desempenho com incorporação de cinzas*. Ph.D. thesis, Escola de Engenharia da Universidade do Minho (in Portuguese) (2002).

Carreira, D. J. and Chu, K. H. "Stress-strain relationship for plain concrete in compression." *ACI journal*, 82(6): 797–804 (1985).

Casanova, P. *Bétons renforcés de fibres métalliques du materiau à la structure*. Ph.D. thesis, Ecole nationale dês Ponts et Chaussées (in French) (1996).

CEB – FIP. *CEB – FIP Model Code 1990, Design code*. Thomas Telford, Lausanne (1993).

Cunha, V. M. C. F. *Análise experimental e numérica do comportamento à tracção de betão reforçado com fibras de aço.* Master's thesis, Universidade do Minho, Guimarães, Portugal (in Portuguese) (2004).

Dramix. "Product data sheet – rc-80/60-bn." Technical report, N.V. Bekaert S.A., Zwevegem, Belgium (1998).

EN 1992-1-1. *Eurocode 2: Design of concrete structures – Part 1 – 1: General rules and rules for buildings.* European Committee for Standardization, Brussels (2004).

Ezeldin, A. S. and Balaguru, P. N. "Normal and high strength fiber reinforced concrete under compression." *Journal of Materials in Civil Engineering*, 4(4): 415–427 (1992).

Grünewald, S. *Performance-based design of self-compacting fibre reinforced concrete.* Ph.D. thesis, TU Delft, Neatherland (2004).

J. Rosenbusch and M. Teutsch. "Shear Design with Method, Test and Design Methods for Steel Fibre reinforced Concrete - Background and Experiences." *Edited by Schnutgen and Vandewalle, RILEM publication PRO 31*, 105–118 (2003).

JSCE – SF4. "Part III – 2 Method of tests for steel fiber reinforced concrete." *Concrete Library of JSCE*, (3): 74 (1984).

Kodur, V. K. R. and Bisby, L. A. "Evaluation of fire endurance of concrete slabs reinforced with fiber-reinforced polymer bars." *Journal of Structural Engineering*, 131(1): 34–43 (2005).

Kooiman, A. G. *Modelling Steel Fibre Reinforced Concrete for Structural Design.* Ph.D. thesis, TU Delft, Neatherland (2000).

L. S. Hsu and C. T. Hsu. "Stress – strain behavior of steel-fiber high strength concrete." *ACI Structural Journal*, 91(4): 448 – 457 (1994).

LNEC E397. "Betões – determinação do módulo de elasticidade em compressão." *Laboratório Nacional de Engenharia Civil* (1993).

Mier, J. V. *Strain-softening of concrete under multiaxial loading conditions.* Ph.D. thesis, University of Delft, Neatherland (1984).

Mier, J. V. *Fracture processes of concrete (Assessment of Material Parameters for Fracture Models).* CRC Press, Boca Raton(FL) (1997).

Montgomery, D. C. and Runger, G. C. *Applied statistics and probability for engineers.* John Wiley & Sons, Inc., Ney York, USA (1994).

Pereira, E. B., Barros, J. A. O., Cunha, V. M. C. F. and Antunes, J. A. B. "Steel fiber reinforced self-compacting concrete for precasted sandwich panels." In "Proocedings ConMat," Vancouver, Canada (2005).

Pereira, E. B., Barros, J. A. O., Ribeiro, A., Cunha, V. M. C. F. and Antunes, J. A. B. "Self compacting steel fibre reinforced concrete for precasted sandwich panels - experimental and numerical research." In "Proocedings BeFib," Ancona, Italy (2004).

RILEM TC 14-CPC. "Modulus of elasticity of concrete in compression (cpc8)." *Materials and Structures*, 6(30) (1975).

RILEM TC 148-SSC. "Strain softening of concrete- test methods for compressive softening, test method for measurement of the strain-softening behaviour of concrete under uniaxial compression." *Materials and Structures*, 33(230): 347–351 (2000).

Ryan, T. P. *Modern regression methods.* John Wiley & Sons, Inc., Ney York, USA (1997).

Annex I

Experimental results

In Tables I.1 and I.2 are indicated the values of the compressive strength obtained for each specimen tested.

Table I.1: Compressive strength values obtained in the *Cf30* series [MPa].

Age	*Specimen*						*Average*
	1	2	3	4	5	6	
12 h	14.12	10.95	12.71	11.50	12.12	-	**12.3**
24 h	22.22	22.96	25.23	26.06	27.36	24.99	**24.7**
3 d	51.27	52.78	52.07	53.26	51.22	53.55	**52.4**
7 d	57.02	59.87	59.18	60.68	57.90	53.70	**58.1**
28 d	69.80	69.97	70.97	67.79	70.69	68.74	**69.7**

Table I.2: Compressive strength values obtained in the *Cf45* series [MPa].

Age	*Specimen*						*Average*
	1	2	3	4	5	6	
12 h	15.32	17.08	17.62	19.43	16.85	19.60	**17.7**
24 h	24.77	23.39	24.75	26.94	25.94	25.85	**25.3**
3 d	48.40	45.86	48.16	49.05	47.63	48.33	**47.9**
7 d	52.86	51.73	54.22	50.56	46.87	49.45	**51.0**
28 d	56.12	54.64	53.58	58.52	55.14	58.90	**56.2**

In Tables I.3 and I.4 are indicated the values of the elasticity modulus obtained for each specimen tested.

Table I.3: Elasticity modulus values obtained in the *Cf30* series [GPa].

Age	*Specimen*						*Average*
	1	2	3	4	5	6	
12 h	12.99	17.87	12.35	11.97	12.74	-	**13.6**
24 h	24.72	27.50	25.10	25.14	25.47	23.68	**25.3**
3 d	36.55	36.57	34.44	37.54	38.24	39.00	**37.1**
7 d	40.72	40.71	40.52	40.37	39.92	40.18	**40.4**
28 d	42.30	40.52	40.15	42.32	41.51	42.17	**41.5**

Table I.4: Elasticity modulus values obtained in the *Cf45* series [GPa].

Age	*Specimen*						*Average*
	1	2	3	4	5	6	
12 h	16.64	18.47	17.92	19.98	19.68	19.88	**18.8**
24 h	21.96	20.82	21.69	24.69	22.69	22.40	**22.4**
3 d	31.30	30.91	32.42	31.20	30.73	31.92	**31.4**
7 d	32.48	32.64	30.95	31.81	31.27	32.26	**31.9**
28 d	34.56	36.55	32.50	35.61	33.22	34.81	**34.5**

In Tables I.5 and I.6 are indicated the values of the elasticity modulus obtained for each specimen tested.

Table I.5: Strain at peak stress values obtained in the *Cf30* series.

Age	*Specimen*						*Average*
	1	2	3	4	5	6	
12 h	0.0094	0.0040	0.0072	0.0068	0.0062	-	**0.0067**
24 h	0.0034	0.0041	0.0037	0.0040	0.0042	0.0037	**0.0039**
3 d	0.0030	0.0031	0.0029	0.0032	0.0029	0.0031	**0.0030**
7 d	0.0034	0.0032	0.0030	0.0030	0.0030	0.0031	**0.0031**
28 d	0.0031	0.0034	0.0032	0.0028	0.0032	0.0031	**0.0031**

In Tables I.7 and I.8 are indicated the values of the energy dissipated under compression obtained for each specimen tested.

Table I.6: Strain at peak stress values obtained in the *Cf45* series.

Age	*Specimen*						*Average*
	1	2	3	4	5	6	
12 h	0.0050	0.0052	0.0044	0.0045	0.0049	0.0039	**0.0047**
24 h	0.0040	0.0039	0.0035	0.0036	0.0038	0.0036	**0.0037**
3 d	0.0031	0.0027	0.0029	0.0030	0.0031	0.0032	**0.0030**
7 d	0.0032	0.0029	0.0031	0.0030	0.0024	0.0029	**0.0029**
28 d	0.0029	0.0029	0.0029	0.0028	0.0029	0.0025	**0.0028**

Table I.7: Energy dissipated under compression values obtained in the *Cf30* series [N/mm^2].

Age	*Specimen*						*Average*
	1	2	3	4	5	6	
12 h	0.30	0.18	0.27	0.28	0.25	-	**0.26**
24 h	0.41	0.33	0.34	0.35	0.43	0.31	**0.36**
3 d	0.55	0.53	0.38	0.47	0.48	0.45	**0.48**
7 d	0.45	0.49	0.54	0.37	0.42	0.38	**0.44**
28 d	0.52	0.56	0.49	0.48	0.41	0.47	**0.49**

Table I.8: Energy dissipated under compression obtained in the *Cf45* series [N/mm^2].

Age	*Specimen*						*Average*
	1	2	3	4	5	6	
12 h	0.29	0.35	0.32	0.27	0.37	0.36	**0.33**
24 h	0.44	0.34	0.33	0.42	0.35	0.37	**0.38**
3 d	0.59	0.49	0.44	0.35	0.37	0.51	**0.46**
7 d	0.63	0.32	0.62	0.40	0.27	0.60	**0.47**
28 d	0.38	0.42	0.28	0.43	0.33	0.48	**0.39**

In Figures I.1 and I.2 is represented the relationship between the dissipated energy under compression and the strain.

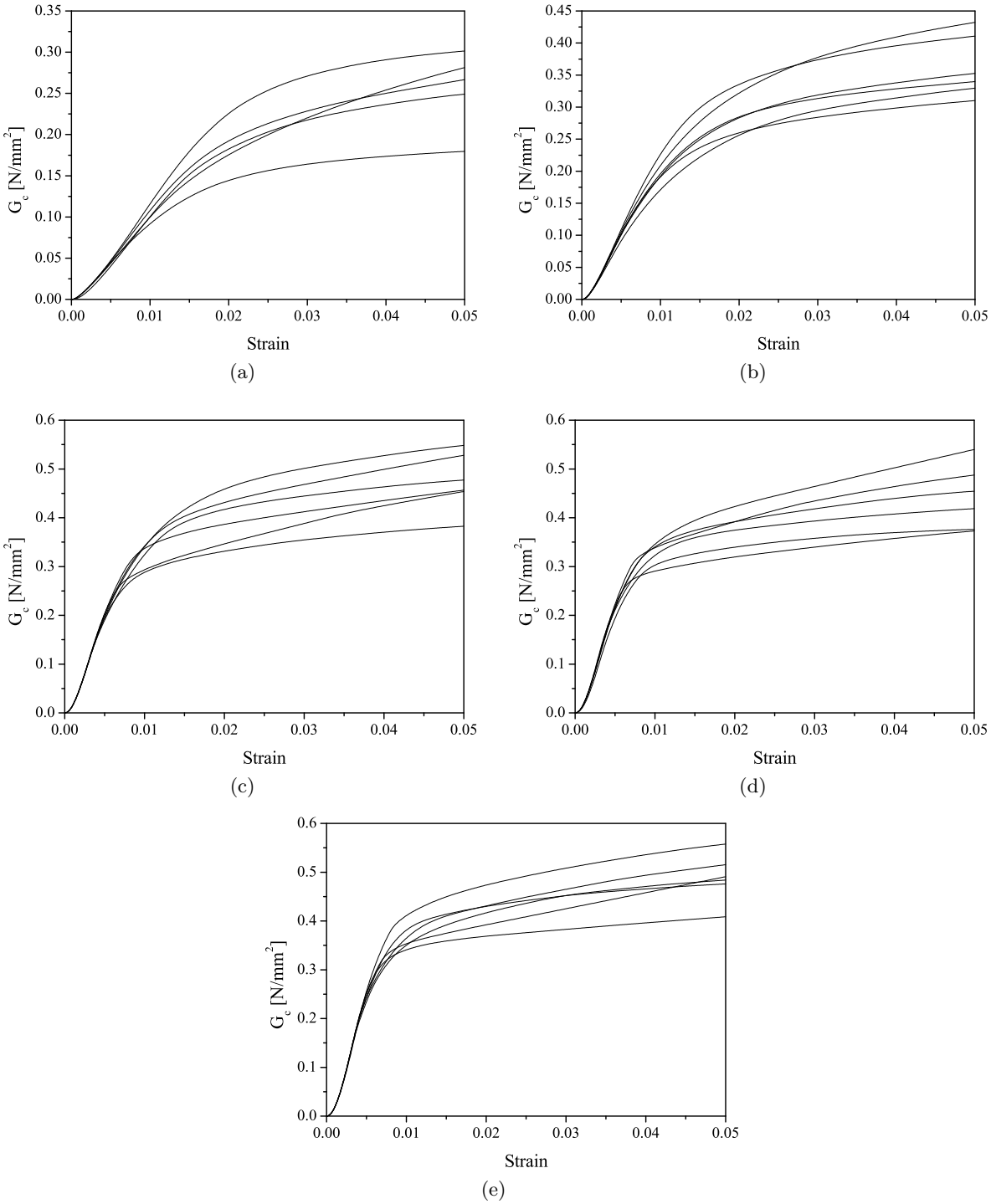

Figure I.1: Relationship between the energy dissipated under compression and the strain for the series *Cf30*: (a) 12 hours, (b) 24 hours, (c) 3 days, (d) 7 days and (e) 28 days.

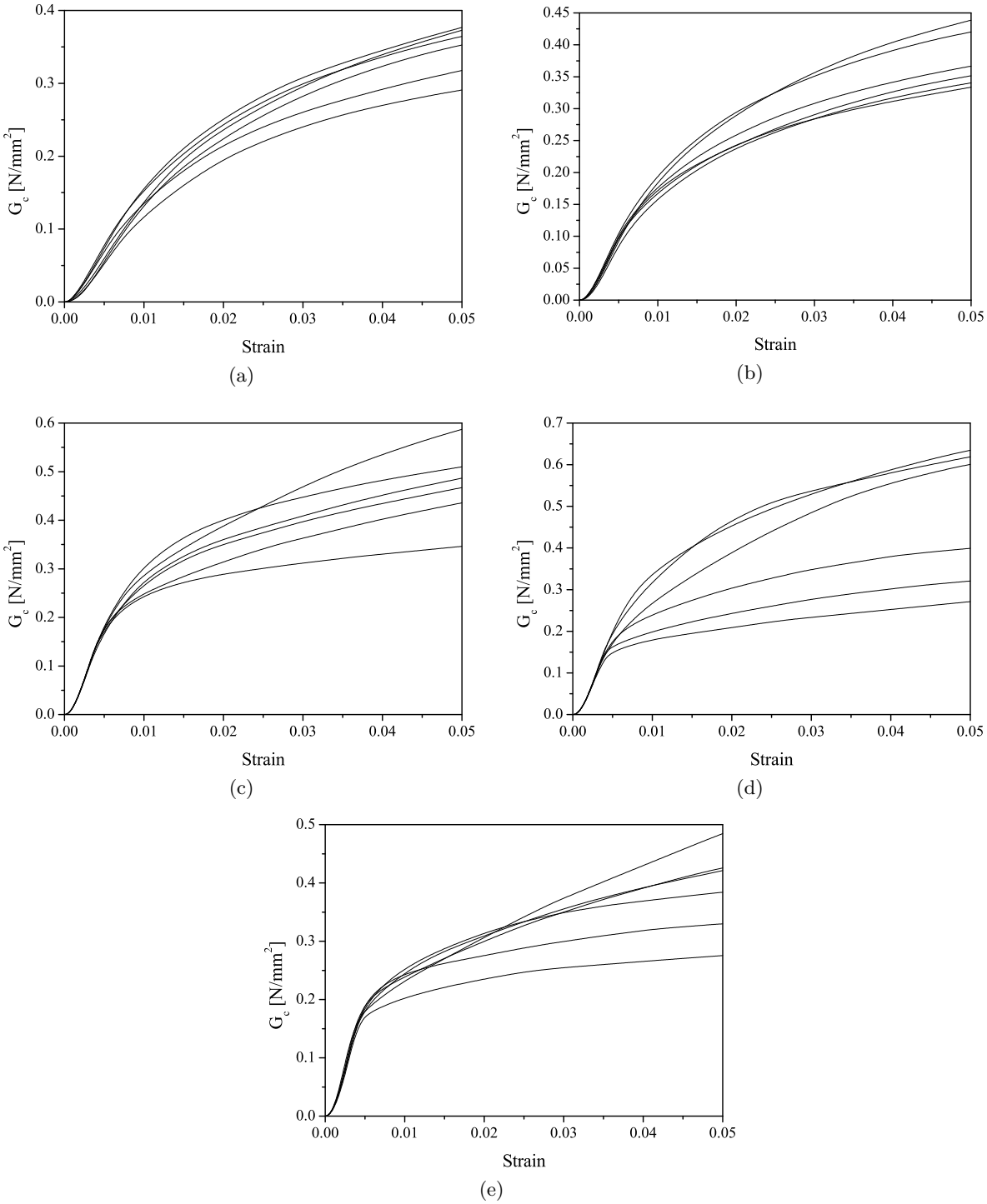

Figure I.2: Relationship between the energy dissipated under compression and the strain for the series *Cf45*: (a) 12 hours, (b) 24 hours, (c) 3 days, (d) 7 days and (e) 28 days.

Annex II

Numerical results

In Table II.1 are indicated the lower-confidence limit (lc) and the upper-confidence limit (uc) values, for the sample with the compressive strength values, whereas in Tables II.2, II.3 and II.4 are indicated, respectively, the (lc) and (uc) values for the samples of the elasticity modulus, strain at peak-stress and energy dissipated under compression.

Table II.1: Confidence limits for the compressive strength.

Age	*Cf30*		*Cf45*	
	lc [MPa]	lc [MPa]	lc [MPa]	lc [MPa]
12 h	10.76	13.80	15.93	19.36
24 h	22.52	26.86	23.98	26.57
3 d	51.31	53.40	46.75	49.06
7 d	55.42	60.69	48.21	53.68
28 d	68.40	70.92	53.89	58.40

Table II.2: Confidence limits for the elasticity modulus.

Age	*Cf30*		*Cf45*	
	lc [MPa]	uc [MPa]	lc [MPa]	uc [MPa]
12 h	10.57	16.60	17.36	20.16
24 h	23.95	26.59	21.00	23.74
3 d	35.38	38.73	30.74	32.08
7 d	40.07	40.73	31.19	32.61
28 d	40.49	42.50	32.97	36.11

Table II.3: Confidence limits for the strain at peak-stress.

Age	*Cf30*		*Cf45*	
	lc	*uc*	*lc*	*uc*
12 h	0.0043	0.0091	0.0041	0.0051
24 h	0.0035	0.0042	0.0035	0.0039
3 d	0.0029	0.0032	0.0028	0.0031
7 d	0.0029	0.0032	0.0026	0.0032
28 d	0.0029	0.0033	0.0026	0.0030

Table II.4: Confidence limits for the energy dissipated under compression.

Age	*Cf30*		*Cf45*	
	lc [N/mm^2]	*uc* [N/mm^2]	*lc* [N/mm^2]	*uc* [N/mm^2]
12 h	0.20	0.31	0.28	0.37
24 h	0.31	0.41	0.33	0.42
3 d	0.41	0.54	0.36	0.55
7 d	0.37	0.51	0.30	0.64
28 d	0.43	0.54	0.31	0.46